

Image-based analyses of morphology and function in the upper airway of orthodontic patients

Xin Feng

Thesis for the degree of Philosophiae Doctor (PhD)
University of Bergen, Norway
2021

UNIVERSITY OF BERGEN



Image-based analyses of morphology and function in the upper airway of orthodontic patients

Xin Feng



Thesis for the degree of Philosophiae Doctor (PhD)
at the University of Bergen

Date of defense: 11.06.2021

© Copyright Xin Feng

The material in this publication is covered by the provisions of the Copyright Act.

Year: 2021

Title: Image-based analyses of morphology and function in the upper airway of orthodontic patients

Name: Xin Feng

Print: Skipnes Kommunikasjon / University of Bergen

This thesis is lovingly dedicated to my family

Table of Contents

SCIENTIFIC ENVIRONMENT	7
SUMMARY	8
LIST OF PUBLICATIONS	10
ABBREVIATIONS.....	12
1. INTRODUCTION	15
1.1 The Adenoid.....	15
1.1.1 Anatomy and physiology	15
1.1.2 Adenoid hypertrophy	16
1.1.3 Clinical symptoms related to adenoid hypertrophy.....	17
1.1.4 Assessment of adenoid hypertrophy	19
1.1.5 Treatment of adenoid hypertrophy.....	20
1.2 Role of dentists in the management of adenoid hypertrophy: assessment and treatment.....	21
1.2.1 Assessment.....	21
1.2.2 Orthodontic treatment	22
1.3 Image-based assessment of upper airway in dentistry	23
1.3.1 2D imaging – lateral cephalogram	23
1.3.2 3D imaging – CBCT	25
1.3.3 3D image-based CFD simulation	28
2. AIMS.....	31
3. MATERIAL AND METHODS	32
3.1 Study design.....	32
3.2 Ethics	33
3.3 Sample collection.....	33
3.4 Imaging.....	34
3.4.1 Lateral cephalogram.....	34
3.4.2 CBCT.....	34
3.5 CFD Simulation	35
3.6 Radiographic and aerodynamic analysis.....	36
3.6.1 Association between AN ratio and morphological parameters	36

3.6.2	Comparison of aerodynamic parameters according to AN ratios.....	38
3.6.3	Comparison of the morphological and aerodynamic changes after RME	39
3.7	<i>Statistical analyses</i>	41
4.	RESULTS	43
4.1	<i>AN ratio Vs morphological characteristics (Study I)</i>	43
4.2	<i>The aerodynamic characteristics according to AN ratios (Study II)</i>	43
4.3	<i>UA morphological and aerodynamic changes after RME (Study III, Study IV)</i>	45
5.	DISCUSSION	49
5.1	<i>Methodology consideration</i>	49
5.2	<i>Interpretation of major findings</i>	50
5.2.1	Lateral cephalogram Vs CBCT	50
5.2.2	Lateral cephalogram Vs CFD simulation	52
5.2.3	CBCT Vs CFD simulation	54
5.3	<i>Clinical implication</i>	56
6.	CONCLUSIONS	58
7.	FUTURE PERSPECTIVES	59
	ACKNOWLEDGEMENTS	60
	References	62
	Original Papers	69

SCIENTIFIC ENVIRONMENT

The studies comprising the thesis were conducted during the years 2017–2021 under the supervision of Professor **Xie-Qi Shi** as main supervisor and Professor **Stein Alte Lie** and Professor **Kristina Hellén-Halme** as co-supervisors. The scientific activities took place at the Department of Clinical Dentistry, University of Bergen, Norway. The imaging data were collected at Dalian stomatological hospital, Dalian, China. The CFD simulation was carried out in collaboration with School of Energy Science and Engineering, Harbin Institute of Technology, Harbin, China.

SUMMARY

Adenoid hypertrophy (AH) is one of the most common causes of nasal obstruction in children and adolescents. This may lead to breathing-related symptoms such as mouth breathing, snoring, asthma, speech problems, and obstructive sleep apnea (OSA). An association between AH and craniofacial abnormalities implies that the initial identification of AH should be an integral part of orthodontic treatment. Moreover, rapid maxillary expansion (RME) has been considered a beneficial tool for reducing nasal obstruction. However, there is currently no consensus on the imaging part of AH diagnosis and how geometrical obstruction due to AH is associated with breathing characteristics. Evidence of both morphological and aerodynamical characteristics of upper airway (UA) is warranted for verifying the effect of RME on UA.

In this thesis, we applied a novel technique, computational fluid dynamic (CFD), to simulate airflow characteristics in orthodontic patients. CFD simulation is a well-established method that uses numerical analysis and data structures to precisely evaluate aerodynamic characteristics of the fluid and their interactions with the surrounding surfaces, as defined by boundary conditions. CFD is widely applied to solve engineering problems, such as in aerospace analysis, weather simulation, and industrial system design, but sparsely used in UA research.

This thesis aimed to validate lateral cephalogram in UA examination using Cone Beam Computed Tomography (CBCT) and CFD simulations. Furthermore, the effect of RME on UA was investigated by CBCT and CFD.

The adenoidal nasopharyngeal (AN) ratios measured on the lateral cephalograms were applied to express the nasopharyngeal airway's adenoidal size and patency. We found a notable correlation ($r = -0.78$) between the AN ratios and the nasopharynx volumes, indicating the higher AN ratio and smaller nasal space in patients 15 years or younger. The CFD simulation demonstrated that the maximal airflow velocity at both inspiration and expiration significantly increased, nearly 30%, once AN ratios were

more than 0.6. With respect to the effect of RME on UA, neither the morphological nor aerodynamic characteristics were significantly changed after RME.

Based on the four studies, we conclude that AN ratios measured on lateral cephalograms could be a feasible method to initially estimate the nasopharynx's patency in children. An AN ratio of more than 0.6 may induce potential alteration in airflow's characters. The utilisation of AN ratios would assist dentists better recognising patients who are at risk of AH. The morphological and aerodynamic changes obtained from CBCT assessment and CFD simulation could not verify the positive effect of RME on UA.

LIST OF PUBLICATIONS

The thesis is based on the following studies and will be referred to according to their Roman numbers:

- I. Xin Feng, Gang Li, Zhenyu Qu, Lin Liu, Karin N Näsström, Xie-Qi Shi. **Comparative analysis of upper airway volume with lateral cephalograms and cone-beam computed tomography.** American Journal of Orthodontics and Dentofacial Orthopedics, 2015. 147(2): p. 197-204. doi: 10.1016/j.ajodo.2014.10.025
- II. Xin Feng, Yicheng Chen, Weihua Cai, Stein Atle Lie, Kristina Hellén-Halme, Xie-Qi Shi. **Prediction of aerodynamic characteristics in the upper airway by the adenoidal nasopharyngeal ratio measured on a lateral cephalogram.** *Submitted manuscript*
- III. Xin Feng, Stein Atle Lie, Kristina Hellén-Halme, Xie-Qi Shi. **The effect of rapid maxillary expansion on upper airway morphology: a retrospective comparison of patients with a normal vs patients with an enlarged adenoid.** Journal of Clinical Pediatric Dentistry, 2021.45(3). doi: 10.17796/1053-4625-45.3.11
- IV. Xin Feng, Yicheng Chen, Kristina Hellén-Halme, Weihua Cai, Xie-Qi Shi. **Effect of rapid maxillary expansion on aerodynamic characteristics of upper airway.** BMC Oral Health, 2021.21(1):123. doi: 10.1186/s12903-021-01488-1

Study I and IV are reprinted with permission from the publisher. All rights reserved.

The author has also contributed to the following work during the course of the PhD period, which is not included in this thesis:

- I. Cecilie Gjerde, Kamal Mustafa, Sølve Hellem, Markus Rojewski, Harald Gjengedal, Mohammed Ahmed Yassin, **Xin Feng**, Siren Skaale, Trond Berge, Annika Rosen, Xie-Qi Shi, Aymen B. Ahmed, Bjørn Tore Gjertsen, Hubert Schrezenmeier & Pierre Layrolle.

Cell therapy induced regeneration of severely atrophied mandibular bone in a clinical trial. *Stem Cell Research Therapy* 2018; 9 (1): 213. doi: 10.1186/s13287-018-0951-9

- II. Yicheng Chen, **Xin Feng**, Xie-Qi Shi, Yijun Zhao, Weihua Cai.

Evaluation of CFD models in predicting airflow characteristics of UA under steady and transient conditions. *Manuscript*

ABBREVIATIONS

AH	Adenoid hypertrophy
AHI	Apnoea hypopnea index
ALADA	As low as diagnostically acceptable
ALARA	As low as reasonably achievable
AN	Adenoid nasopharyngeal
CBCT	Cone beam computed tomography
CFD	Computational fluid dynamics
CSA	Cross-sectional area
DICOM	Digital imaging and communications in medicine
ENT	Ear, nose, and throat
HIV	Human immunodeficiency virus
ICC	Intraclass correlation coefficient
kV	Kilovolt
RME	Rapid maxillary expansion
mA	Milliampere
mL	Milliliter
MRI	Magnetic resonance imaging
MSCT	Multi-slice computed tomography

Pa	Pascal
P_{ws}	Wall shear stress
P_w	Wall static pressure
OME	Otitis media with effusion
OSA	Obstructive sleep apnoea
s	Second
SDB	Obstructive sleep- disordered breathing
T0	Baseline pre-treatment
T1	Post-treatment
UA	Upper airway
V_{ms}	Midsagittal velocity
2D	Two-dimensional
3D	Three-dimensional
ΔP	Pressure drop

1. INTRODUCTION

1.1 The Adenoid

1.1.1 Anatomy and physiology

In 1661, Schneider [1] first described that adenoid originated from the mucus lining the nose, not the pituitary and brain. In current medicine, adenoid is defined as a mucosa-associated lymphoid tissue, also known as the pharyngeal tonsil or nasopharyngeal tonsil. The adenoid originates from the pharyngeal endoderm in the posterior midline of the nasopharynx, which is a pyramidal-shaped structure attached to the roof of the pharynx with the apex towards the nasal septum and the base on the posterior wall of the nasopharynx. The specific arrangement of the lymphoid tissue in the pharynx was first described by Waldeyer in 1884 [2]. Adenoid constitutes the Waldeyer's ring in conjunction with the tubal tonsil, palatine tonsil, and lingual tonsil. The paired tubal tonsils are situated at the pharyngeal openings of the eustachian tubes; the paired palatine tonsils are located in the oropharynx; and the lingual tonsils are on the posterior of the tongue [3] (**Figure 1**). As the superior-most lymphoid tissue of the Waldeyer ring, adenoid is the first immune system's line of defense against foreign pathogens through the respiratory tract [4, 5]. In childhood, the adenoid size coincides with the immunologic response for constructing the integral immune system [6, 7].

The physical development of adenoid starts from the fetal period and is usually visible in infants aged six months [8]. It grows rapidly up to age two years, almost occupies the half-space of the nasopharynx, and follows with a growing peak at age four years, then progressively shrinks until 15 years. By adulthood, the adenoid almost completely atrophies [9].

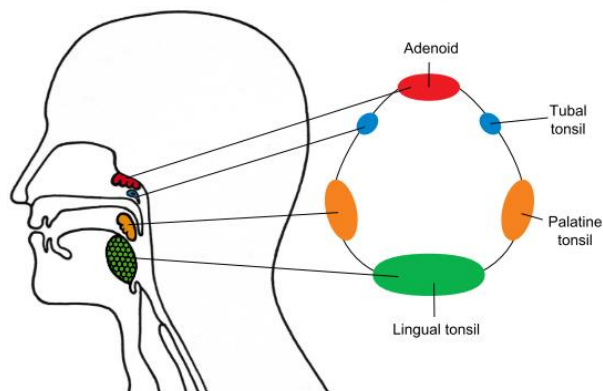


Figure 1. Illustration of Waldeyer ring. Adapted from [3].

1.1.2 Adenoid hypertrophy

The prevalence of adenoid hypertrophy (AH) was markedly variable with respect to age and country [10-15]. The prevalence of 34% has been reported in a randomised representative sample recruited from primary school [16]. It is well accepted that the adenoid has its growth spurt from birth to four years, and then sharply diminished after 12 years [9]. However, the adolescents aged 11 to 14 years old only had a slightly lower prevalence of AH, 19.9% compared with 27.0% in those aged 5–7 years, and it was almost equal to those aged 8–10 years (19.5%) [17]. As such, AH occurring in adolescents should not be ignored in clinics.

During the childhood and adolescence period, both infectious and non-infectious etiologies can lead to AH. The bacteria and viruses enter through the respiratory tract and can cause respiratory infections [18, 19]. The adenoid and palatine tonsils are the most responsive lymphoid tissues on the pharynx and start the immune process [20]. The palatine tonsils are more often mentioned than adenoid in the process of respiratory infection by parents and clinicians because the palatine tonsils are easily investigated through the mouth, whereas the adenoid is invisible. Besides, palatine tonsils are situated on both sides of the back of the throat, and enlarged palatine tonsils may result

in a sore throat which is often a cause for complaint, but the obstructive symptoms caused by an enlarged adenoid such as a stuffed-nose and mouth breathing are often ignored.

Palatine tonsils and adenoids usually return to normal size once the infection is gone. However, recurrent or chronic infections may result in pathological diseases. Apart from infectious reasons, severely allergic diseases such as asthma, allergic rhinitis, and atopic dermatitis occurring in children may be other potentially impacted factors [21]. Allergic rhinitis has been reported as one of the most common allergic conditions that simultaneously occurs with AH [22]. Also, the living environment is an important factor for AH's presence as well. The house dust mite has been considered as the most common allergens in patients with AH; in addition, parental smoking within the household was another risk for AH occurrence [22].

For adults, AH may be a more serious indication of human immunodeficiency virus (HIV) infection [3], lymphoma, or sino-nasal malignancy, although the occurrence of AH was much lower in adults than children and adolescents.

1.1.3 Clinical symptoms related to adenoid hypertrophy

AH may cause various symptoms such as otitis media with effusion (OME), obstructive nasal breathing, hypo nasal voice [23], and specific facial morphology. The symptoms are highly dependent on the degree and duration of the AH; mild and moderate obstruction may thus not be a cause for complaint by children nor observed by parents or caregivers, and this may, in turn, result in chronic pathological diseases such as obstructive sleeping.

AH is a common cause for OME in childhood [24], as the opening of the eustachian tube on the nasopharyngeal wall is in proximity to the adenoid. The enlarged adenoid may extend towards the opening of the eustachian tube and block it, leading to eustachian tube dysfunction, abnormal ventilation of the middle ear, and hearing loss in children [25]. Except for the physical obstruction caused by AH, a regional inflammatory reaction in the eustachian tube and middle ear may also be caused by the release of inflammatory mediators i.e., adenoid mast cells [26].

One of the most severe symptoms associated with AH is obstructive sleep disordered breathing (SDB), which is defined as a syndrome of upper airway (UA) dysfunction caused by partial or complete UA obstructions during sleep. The clinical symptoms range from mild snoring to severe obstructive sleep apnoea (OSA). For adults, OSA contributes to an increased risk of coronary artery disease, congestive heart failure, myocardial infarction, hypertension, stroke, cardiac arrhythmia, and sudden cardiac death [27-29]. Compared to adults, there is less morbidity and mortality related to children [30]. There are specific symptoms reported by parents or caregivers, such as snoring or spontaneous arousals during sleep, and by teachers including daytime sleeping, reduced cognitive function, and academic performance [30, 31].

The little known effect of AH is that it may adversely force nose breathing into mouth breathing. In comparison with nose breathing, mouth breathing results in a lower tongue position, lower mandibular position, and extended head posture [32]. Leaving the symptoms unrecognised and AH undiagnosed, the abnormal breathing mode may affect the maxillofacial growth. The children and adolescents who have enlarged adenoids may show specific facial characters, such as a high and narrow upper dental arch, increased anterior face, and retrognathic mandible known as the adenoid face [33-36] (**Figure 2**). The specific craniofacial morphologies may in turn increase children's risk for having OSA [37]. Therefore, it was recommended by the American Association of Orthodontists in 2019 that the evaluation for OSA in every child should be a part of an orthodontist's comprehensive clinical assessment [38].



Figure 2. Patients with adenoid facies before and after operation, from Dr. Meyer's publication of November 4, 1868. adapted from [39].

1.1.4 Assessment of adenoid hypertrophy

Since the medical community recognised and adopted Meyer's discovery [36], numerous improvements in AH diagnosis have been developed worldwide [39]. The adenoid is invisible on direct inspection, and several modalities have been applied to investigate adenoids in otolaryngology clinics, such as rhinomanometry [40], acoustic rhinometry [41, 42], and endoscopy [43] (**Figure 3**). Among these examinations, nasal endoscopy is the only technique to make the adenoid visible, and it is accepted by ear, nose, and throat (ENT) experts as the standard reference for diagnosing AH [44]. However, as an invasive examination, endoscopy is challenging to perform on non-cooperative children. Imaging examinations are thus widely accepted for observing the adenoid; the lateral cephalogram has been commonly performed on children suspected of having AH.

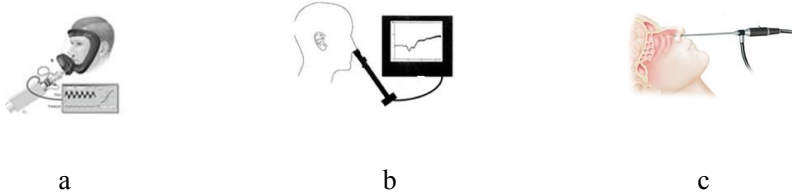


Figure 3. Clinical examination. (a) rhinomanometry, adapted from [45]; (b) acoustic rhinometry, adapted from www.aibolita.com/surgical-treatment/54104-theory-of-acoustic-rhinometry.html; (c) endoscopy, adapted from www.saintlukeskc.org/health-library/understanding-endoscopic-endonasal-surgery.

Generally, a lateral cephalogram combined with a clinical assessment is relatively sufficient to assess adenoid hypertrophy. Multi-slice computed tomography (MSCT) and Magnetic resonance imaging (MRI) are only used in selected patients due to the higher radiation doses (MSCT) and cost (MSCT/MRI) compared to lateral cephalograms. A few retrospective studies investigated the adenoid on MSCT and MRI images [46-49], reporting that three-dimensional (3D) imaging provided much more anatomic details and demonstrated the relationship between the adenoid and the surrounding tissues. Furthermore, based on 3D imaging, functional characteristics related to adenoid could be demonstrated by applying specific diffusion-weighted imaging or dynamic simulation [50, 51]. In short, 3D imaging modalities may lead to a start towards the functional evaluation on patients with AH.

1.1.5 Treatment of adenoid hypertrophy

Non-surgical treatment

For children with mild or moderate symptoms without specific syndromes, watchful waiting with supportive care has been the main approach considered by both parents and clinicians [52]. The non-surgical treatments for AH were highly dependent on the multiple etiologies. Antibiotic therapy [53], intranasal corticosteroid [54], and Chinese herbal medicine [55] have been used for AH's treatment.

Surgical treatment

In 1868 the Danish physician Meyer [36] first described the AH related nasal obstruction which may lead to mouth breathing, snoring, abnormal facial development, otitis, and speaking problem. Meanwhile, he suggested removing the adenoids surgically to treat the clinical symptoms. Adenoidectomy with or without tonsillectomy currently remains the most frequently performed surgical procedure in children. A considerable variation was reported between countries regarding the incidence of adenoidectomy in children in the past twenty years. In the United States, the incidence of adenoidectomy was 1.76/1000 children in 2006 [56]. The number was up to 13.3/1000, 4.4/1000 in Finland and Norway in 2005, respectively [57], and 7.4 /1000 in another Northern European country, Sweden, during 2004–2013 [58].

Common indications of early adenoidectomy are recurrent UA infections and otitis media [57]. Following the recent recognition of AH related pediatric OSA, the adenoidectomy is more frequently performed for decreasing the degree of obstruction [59, 60]. However, besides the operative risk and postoperative complications [61], the removal of adenoid tissue may have a negative impact on immune function. The long-term risk of respiratory, allergic, and infectious diseases after adenoidectomy has been under consideration [62]. Hence, the necessity of surgery has been questioned for children with mild or moderate AH [52, 63].

1.2 Role of dentists in the management of adenoid hypertrophy: assessment and treatment

1.2.1 Assessment

Generally, the AH diagnosis is determined by ENT specialists. However, it is important to note that orthodontists should also be involved, as the specific morphological abnormalities during early growth are closely associated with obstructive nasal breathing [34, 64, 65]. On the other hand, ignoring such interactions between breathing conditions and maxillofacial morphology, by solely focusing on correcting the visually recognisable maxillofacial abnormality, may result in inadequate and limited

orthodontic treatment [66]. Due to the complex causes for AH and various symptoms induced by AH, a multidisciplinary team of specialists, including otolaryngologists, pediatricians, and orthodontists has been suggested for managing children with suspected adenoidal obstruction to define the most appropriate diagnostic and therapeutic options for individuals [38, 67].

For orthodontists, it is thus important to identify the patients with AH further in order to recognise the maxillofacial morphology related to obstructive breathing. A further ENT assessment may be recommended to prevent the development of serious maxillofacial abnormality or the later OSA. For this purpose, an easily acceptable and highly valid screening method is warranted for AH estimation on available imaging data for both orthodontics and oral radiologists.

1.2.2 Orthodontic treatment

Rapid maxillary expansion (RME) has been widely used to increase the transverse dimensions of the maxillary arch in patients with narrow maxilla (**Figure 4**). Some orthodontists suggested RME may increase the nasal space and then improve the nasal obstruction after opening the midsagittal suture, separating the two maxillas, and expanding the maxillary width [66, 68]. RME mainly increases the maxilla width in the transverse direction, and the skeletal boundary of the nasal cavity was directly extended following the expanded maxilla. However, the influence of RME on the pharynx is disputed since it locates posteriorly to the maxilla and is surrounded by multiple soft tissues.

Also, physical growth plays a role in the choice of appropriate treatment, as the nasopharyngeal skeleton and nasopharyngeal lymphoid tissue have their age-dependent development [69]. Cohen et al. [49] revealed that the narrowest airway occurred in the age group of 5.1–8 years when the growing speed of adenoid was faster than bony nasopharynx. After eight years, the adenoid atrophies while the bony nasopharynx continues to grow, resulting in the broader airway and reductive obstruction.

The natural development of the nasopharynx may indicate an age-dependent treatment, that is, an adenoidectomy may be recommended for children younger than eight years. For children older than 8 years having narrow maxilla, the increased nasopharyngeal space resulted from RME may also improve nasal breathing. So far, no consensus has been achieved, and more evidence is warranted for affirming the positive effect of RME on obstructive UA caused by AH.



Figure 4. RME procedure. A fixed Hyrax expander is banded to the maxillary first premolars and first molars. The patient, or their guardian, rotate the expansion screw twice a day at home and a clinical check-up is performed by orthodontists once a week. The expansion is terminated when the occlusal aspect of the maxillary lingual cusps of the upper first molars contacted the occlusal aspect of the vestibular cusp of the mandibular first molars.

1.3 Image-based assessment of upper airway in dentistry

1.3.1 2D imaging – lateral cephalogram

Lateral cephalogram, a profile X-ray of the head and neck, is the most commonly used radiographic method for assessing AH in ENT clinics. On the other hand, lateral cephalogram is a widely applied radiographic method performed on children prior to orthodontic treatment for assessing the characteristic malocclusion, tracing the anatomic landmarks, and overviewing the skeletal structure. As such, the imaging material is usually already available for investigating adenoids for orthodontic patients.

Although the accuracy of lateral cephalograms for investigating AH has been verified by rhinometry or operational examination [70, 71], the low specificity and low correlations with endoscopic evaluation have also been reported [72-77]. The various measuring protocols on lateral cephalograms may lead to inconsistent conclusions regarding the applicability of lateral cephalograms for diagnosing AH. Several parameters have been used for assessing the adenoid and nasopharynx on lateral cephalograms such as the distance, area, and ratio of the adenoid and nasopharynx [71, 78-80]. As the obstructive degree is dependent on both the adenoid size and the nasopharyngeal width, the sole assessment of the adenoid or nasopharynx can not efficiently express the obstructive upper airway.

The relationship of the adenoid to the nasopharyngeal airway could be represented by the adenoid nasopharyngeal (AN) ratio measured on lateral cephalogram, first described by Fujioka et al. [9] (**Figure 5**). The AN ratio was calculated by two linear measurements presenting the size of the adenoid and nasopharynx, respectively. Over the years, many studies applied the original Fujioka's method or a modified method for measuring the AN ratio [81-84]. The AN ratio exhibited a significant correlation with the volume of adenoid removed at operation [85] and with nasal endoscopic examination findings [83, 86]. Soldatova et al. [87] concluded that AN ratio of 0.65 could be used for estimating a moderate nasopharyngeal obstruction based on the observation during intraoperative mirror examination. An adenoidectomy has been recommended by clinicians at a threshold AN ratio of 0.73 [84]. However, the AN ratio has not been well known by dentists, and it may be a simply feasible approach to identify orthodontic patients who are at risk of AH.

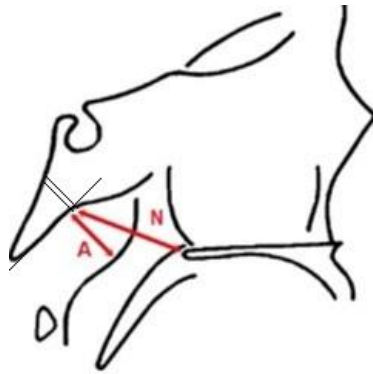


Figure 5. AN ratio measurements: A – indicates adenoid thickness; N – indicates the nasopharyngeal width. adapted from [86].

1.3.2 3D imaging – CBCT

Justification and optimization of x-ray examinations

X-ray is widely applied in medical diagnoses and treatment. Due to the potential radiation risk associated with x-ray exposure, justification and optimization of x-ray examination are particularly important, especially for children, because of their greater radiation risk. The ALARA principle [88], as low as reasonably achievable, has been adapted upon over time by specifying the importance of the dose exposure being as low as diagnostically acceptable (ALADA) [89]. Therefore, when a new radiological modality emerges, its diagnostic benefit and radiation risk shall be evaluated and compared with conventional methods.

3D imaging provides more extensive and detailed information for demonstrating the UA morphology in multiplanes as well as volumetric rendering model, but at the expense of higher radiation doses than traditional two-dimensional (2D) imaging. 3D x-ray examination of UA needs to be justified by considering whether the obtained information is crucial for diagnosis and the follow-up treatment choice.

CBCT

CBCT was introduced in dentistry by Mozzo et al. in 1998 [90], specifically designed for dental maxillofacial imaging. CBCT has gained growing popularity among dentists due to the ease of acquisition and impressive 3D reconstruction with high spatial resolution. CBCT entails a lower radiation dose than MSCT [91] but increased radiation risk compared to conventional radiographs, such as lateral cephalogram. So far, CBCT has become an easily accessible radiological modality for dentists and is widely applied in various diagnostic task, such as for bone assessment prior to implant treatment. Compared to MSCT, CBCT images provide higher spatial resolution due to their small isotropic voxels but lower contrast resolution, and thus unsuitable for soft tissue diagnostics. Despite CBCT being inferior to MSCT in discriminating between different soft-tissue structures, the high anatomical contrast between soft tissues and air makes it possible to define the boundary of UA. CBCT is thus now considered to be an effective and accurate alternative to MSCT for investigating UA [92-95].

On CBCT images, the UA may be divided into four regions. The start region is the nasal cavity, followed by the nasopharynx, where the adenoid situates. The next part is the oropharynx including the soft palate and tonsils, and the last region is the hypopharynx or laryngopharynx. The area or volume of each region could be automatically obtained while the boundary is defined by applying software (**Figure 6**).

There has been a number of reports on the clinical application of CBCT on patients who underwent mandible setback surgery, mandible advancement treatment, or rapid maxillary expansion [96-99]. The changes of UA morphology caused by these treatments may be detected on images as these specific patients already had the CBCT images available since 3D information is required for diagnostic indication.

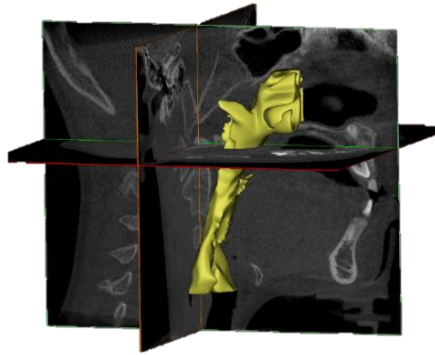


Figure 6. UA segmentation on CBCT images.

When applying CBCT images for an investigation of the adenoid size, high sensitivity of 88% and specificity of 93% for diagnosing AH has been reported by Major et al. [100]. It is of interest to note that even on the 3D images, they used a 2D parameter to grade the AH related nasal obstruction by calculating the percentage of adenoid occupied the nasopharynx. Other researchers have also tried to seek a 2D parameter on a lateral cephalogram representing the 3D morphology of the UA [101, 102], in which the most efficient 2D parameter was the nasopharyngeal area measured on lateral cephalograms. The larger area indicated the larger nasopharyngeal volume; however, defining the area on lateral cephalograms was time-consuming. So far, an efficient 2D parameter for estimating 3D UA morphology has not been achieved. AN ratio has not been associated with 3D morphology in previous studies.

One question is notable, namely, does the morphological characters demonstrated on CBCT images reflect the functional features of UA? The limited availability of functional tools makes respiratory assessment impossible for dentists. As mentioned earlier, the changes of UA morphology related to orthognathic surgery or orthodontic treatments have been investigated employing CBCT images, and very few studies associated the morphological changes to the respiratory function in terms of oxygen saturation [103], apnoea hypopnea index (AHI) [104], and clinical symptoms.

Assessment of UA morphology in relation to respiratory function is essential in targeting patients having potential UA obstruction, and may further be applicable for predicting the outcome of treatment. Although there is a critical requirement for understanding the image based geometry-property related to the UA function, unfortunately, the current state of information obtained from imaging can not provide the answer.

In summary, two main questions need to be addressed with respect to investigating adenoid on images. Can a 2D parameter measured on lateral cephalogram be used for estimating the 3D morphology of UA? Secondly, does the morphology of UA demonstrated on images associate with the functional features of UA?

1.3.3 3D image-based CFD simulation

What is CFD?

Computational fluid dynamics (CFD) is a well-established technique for simulating fluid motion using numerical algorithms, which has been widely used in mechanical engineering for years. After designing a virtual model, the aerodynamic characteristics such as the pressure, velocity, and flow patterns can be simulated and calculated without the high costs associated with experimental analyses. Consequently, CFD plays an ever-growing role in the field of medicine, by applying CFD approach the human's anatomic structure can be investigated as a biomechanical model e.g., blood vessels.

Application in medicine

The CFD has been utilised for the demonstration and assessment of biomedical procedures in medicine. The most notable application was in cardiovascular systems. Based on medical 3D images, the advent of CFD made the complex transport phenomena feasible i.e. blood flow in vessels or airflow in airways. As the biomechanics between anatomical structure and the functional feature can be investigated using CFD simulation, many challenging and clinically relevant problems could be explained by aerodynamic characteristics. One of the aerodynamic parameters

wall shear stress was found to be closely associated with aneurysm geometry, which pointed out the relationship between wall shear stress and aneurysm rupture (**Figure 7**). The higher wall shear stress may indicate a thinner aneurysm wall [105], and the higher wall shear stress may also predict the location of the aneurysm rupture [106].

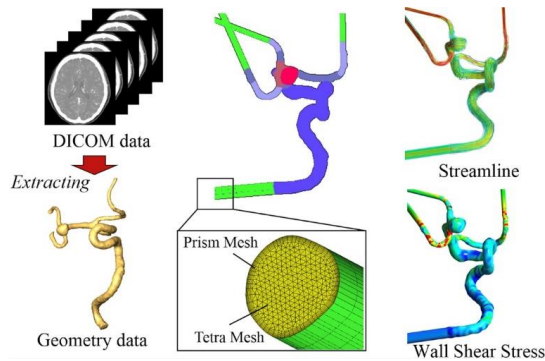


Figure 7. CFD analysis of aneurysm data. adapted from [107]

Regarding the field of dentistry, most CFD studies focus on nasal respiratory function after orthognathic surgery, orthodontic treatment, and OSA therapy. Kita et al. [108] reported that bimaxillary orthognathic surgery could increase the cross-sectional area of nasal cavity, where the pressure tended to decrease accordingly. Iwasaki et al. also [109] found an improvement in nasal ventilation after RME by CFD simulation. The outcome of the mandibular advancement device, as well as the distraction osteogenesis maxillary expansion for treating OSA, has been confirmed by CFD simulation, demonstrating a reduction in airflow obstruction in terms of velocity and pressure [110-112]. Through CFD simulation, these previous studies showed that UA's anatomical geometry was associated with airflow properties. Zhao et al. [113] stated that the geometric changes alone did not correlate well with treatment response, and they supported CFD as a potential tool for the prediction of treatment outcome in OSA patients. However, when to apply CFD simulation and how to construct a CFD model are still under debate as the CFD simulation is a complex procedure and very skill-dependent. In the meantime, there are still some challenges in CFD clinical application,

for instance, the definition of boundary conditions, the choice of a representative parameter, and the setting of respiratory phases.

Considerations for CFD aiding UA assessment

Due to the utilisation of CFD in the assessment of UA in the literature, CFD may be used as a bridge for linking the adenoid-related UA obstruction and airflow functional characteristics. To our knowledge, only one published study detected the relationship between AH and the airflow features, in which the maximum negative pressure was found correlated with the minimum cross-sectional area (CSA) obtained on CT images [114]. However, the 2D parameter on lateral cephalograms has not been quantitatively associated with airflow dynamic characteristics by means of CFD. As lateral cephalogram is more readily available for orthodontic patients with considerably lower radiation risk than CT or CBCT; thus it is essential to validate whether lateral cephalogram can be applied to estimate the 3D morphology and the function of UA focusing on adenoid.

2. AIMS


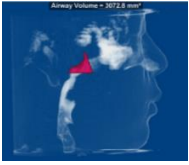

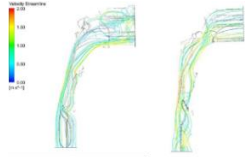

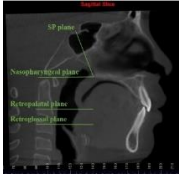

The overall aim of this thesis was two-fold: first to validate lateral cephalogram in AH diagnostics using CBCT and CFD simulation. Secondly, the effect of RME on UA was investigated by CBCT and CFD.

Specific aims were:

- To evaluate whether the AN ratio on lateral cephalograms could be used to estimate the airway volume, using CBCT as the validation method (Study I).
- To investigate the aerodynamic characteristics within UA on orthodontic patients employing CFD simulation. Furthermore, airflow features were compared between normal and patients suspected of having AH (Study II).
- To evaluate the effect of RME on the morphology of the UA in patients with and without AH (Study III).
- To evaluate the outcome of RME on the UA function in terms of aerodynamic characteristics by applying a CFD simulation (Study IV).

3. MATERIAL AND METHODS

3.1 Study design

Study	Applied methods		Calculated parameters
I	 <p data-bbox="288 706 484 733">Lateral cephalogram</p>	 <p data-bbox="667 706 723 733">CBCT</p>	<ul data-bbox="906 476 1012 556" style="list-style-type: none"> • AN ratio • Areas • Volumes
II	 <p data-bbox="288 979 484 1006">Lateral cephalogram</p>	 <p data-bbox="672 979 718 1006">CFD</p>	<ul data-bbox="906 749 1102 986" style="list-style-type: none"> • AN ratio • Pressure drop (ΔP) • Maximum midsagittal velocity (V_{ms}) • Maximum wall shear stress (P_{ws}) • Minimum wall static pressure (P_w)
III		 <p data-bbox="667 1223 723 1250">CBCT</p>	<ul data-bbox="906 1031 1012 1112" style="list-style-type: none"> • AN ratio • Areas • Volumes
IV	<p data-bbox="363 1488 414 1516">RME</p>	 <p data-bbox="672 1488 718 1516">CFD</p>	<ul data-bbox="906 1264 1102 1403" style="list-style-type: none"> • Pressure drop (ΔP) • Maximum midsagittal velocity (V_{ms}) • Maximum wall shear stress (P_{ws})

All four included studies were retrospective studies aiming to evaluate the UA condition in terms of morphology and aerodynamics using the available imaging materials of the orthodontic patients. **Study I and Study II** were retrospective observational studies for investigating whether the 2D parameter obtained from the lateral cephalogram i.e. AN ratio, could be used to estimate the UA morphology and aerodynamics of UA. **Study III and Study IV** were retrospective cohort studies to evaluate the effect of RME on UA by means of CBCT images and CFD simulation.

3.2 Ethics

The studies I–IV were approved by the ethics committee of China as well as the ethics committee of Norway: Study I (DLKQLL201302, Dalian Stomatological Hospital, China) and Studies II, III, IV (DLKQLL201604, Dalian Stomatological Hospital, China; 2018/1547 REK Vest, University of Bergen, Norway). The samples were collected following informed consent of the patients.

3.3 Sample collection

All the data were retrospectively collected at the Department of Orthodontics, Stomatological Hospital, Dalian, China between 2010 and 2016. The database was searched systematically.

The inclusion criteria were cases with one lateral cephalogram and one CBCT scan examined within one week. All the radiographs were taken prior to the start of the treatment due to various orthodontic reasons. For CBCT scans, the field of view should cover the whole upper airway including the nasal cavity, nasopharynx, and oropharynx. The exclusion criteria were severe abnormalities of maxillofacial tissue, previous surgery on skeletal and soft tissue related to respiration, and previous orthodontic or orthopaedic treatment. All the scans were previewed, and images with motion artifacts and suboptimal patient positing were excluded.

The inclusion criteria in Study II included cases aged 9 to 15 years. Specific inclusion criteria in Study III and Study IV were cases younger than or equal to 15 years and CBCT scans had been performed pre- and post-RME (**Figure 8**). The pre-RME CBCT scans were made in the seven days before cementation of the expander (T0), and the post-RME CBCT scans were taken at the end of the retention phase (T1).

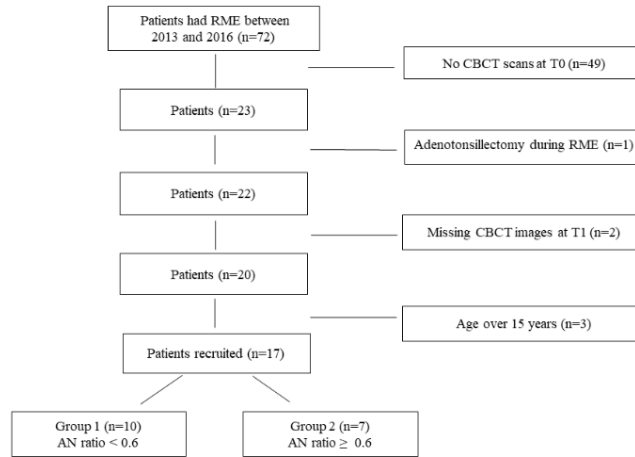


Figure 8. Flowchart of patient selection in Study III and Study IV.

3.4 Imaging

3.4.1 Lateral cephalogram

A Digital Pan/Ceph System (ORTHOPHOS XG 5, Sirona, Germany) was used at 73 kVp, 15 mA with an exposure time 9.4 seconds. The magnification factor is 1.1 with a 16 bit pixel depth for all the images.

3.4.2 CBCT

One CBCT device (3D eXam; KaVo, Biberach an der Riss, Germany) was applied at 120 kV and 5 mA, with a scanning time of 14.7 seconds for the patients according to the manufacturer's guidelines. The voxel size was 0.2 mm, with 14-bit pixel depth for all the images, and the field of view varied depending on the purpose of the

examination. CBCT scans followed standardised clinical routines, that is, with the Frankfort horizontal plane parallel to the floor, the teeth in maximum intercuspation, and the patient breathing calmly with no swallowing.

3.5 CFD Simulation

The CBCT images were imported to MIMICS software (23.0 MIMICS, Materialise, Belgium) in the digital imaging and communications in medicine (DICOM) format for later analysis. 3D renderings of the CBCT scans were oriented with axial planes paralleling the Frankfurt horizontal plane; the midsagittal planes intersected the nasion and anterior nasal spine; and the coronal plane was adjusted to the level of the porions. For each case, a mask was reconstructed, making sure the integrity of UA was displayed correctly. CFD simulation was then conducted on the 3D model within the mask region. The superior boundary of the studied UA was defined as a vertical plane, in the nasal cavity, passing through the most posterior point of the middle turbinate, whereas the inferior boundary was a horizontal plane, in the pharynx, in line with the most anterior-inferior point of cervical vertebra 4. Each end of the boundary was extended by 20mm to avoid flow reversing during the simulating process. The inlet and outlet of UA were set at the extended planes. A surface model was then created according to the extended 3D model for mesh generation by ANSYS ICEM (ANSYS, Inc., Canonsburg, Pennsylvania). The inlet and outlet at the surface of UA were defined. Each UA mesh was with five boundary layers and an average of 2 million elements in a size of 0.6. ANSYS Fluent (ANSYS, Inc., Canonsburg, Pennsylvania) was applied to calculate the aerodynamics characteristics during the respiratory circle. The boundary condition of UA was set. In the inspiratory phase, the inlet of UA was set with pressure 0 Pa and the outlet of UA with a flow rate of -200 mL/s. The corresponding values were -200 mL/s and 0 Pa at inlet and outlet for the expiratory phase.

3.6 Radiographic and aerodynamic analysis

3.6.1 Association between AN ratio and morphological parameters

To detect the association between AN ratio and the UA morphology in terms of areas and volumes of the nasopharynx and total upper airway, 55 participants were classified into two groups according to age: group A (≤ 15 years) and group B (> 15 years).

AN ratio measurement

The AN ratio as the ratio of the thickness of the adenoid to the width of the nasopharynx was measured on the lateral cephalograms [115]. A denotes the perpendicular distance between the points of maximal convexity of the adenoid shadow and the anterior margin of the basiocciput, while N denotes the distance between the posterosuperior edge of the hard palate and the anteroinferior edge of the spheno-occipital synchondrosis (**Figure 9**).

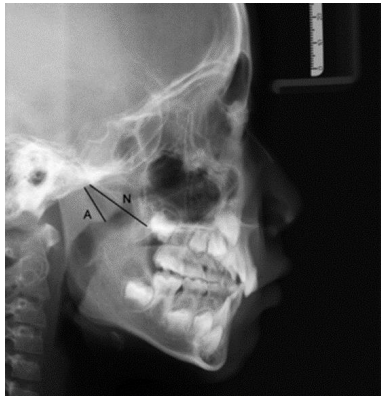


Figure 9. Calculating the adenoidal nasopharyngeal (AN) ratio. A – Perpendicular distance between maximum convexity of the adenoid shadow and the anterior margin of the basiocciput; N – Distance between the posterosuperior edge of the hard palate and the anteroinferior edge of the spheno-occipital synchondrosis.

The morphological assessment

The areas and volumes of UA were calculated by applying 3D airway reconstruction. The CBCT images were imported as DICOM data to imaging software (Dolphin Imaging & Management Solutions, Chatsworth, Calif). Once the image was properly oriented, the software created a 2D simulated lateral cephalometric image at the midsagittal plane. From this view, the nasopharyngeal UA was defined with the superior border at a line connecting the midpoint of sella turcica and the posterior nasal spine, and with the inferior border at a line connecting the point most posteroinferior on the clivus with the posterior nasal spine. For the total UA, the superior border was the same as the nasopharynx, and the lower border of the airway was defined at a horizontal level with the tip of the epiglottis against the wall of the posterior airway. Data of area and volume in the midsagittal view could be calculated and presented automatically once the boundary of the airway was defined (**Figure 10**).

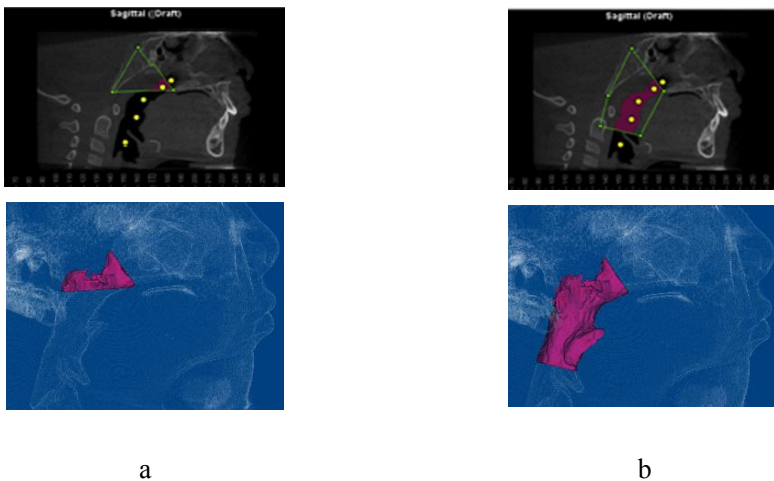


Figure 10. The area and volume was calculated and presented after the boundaries were defined from the sagittal view: a – nasopharynx; b – total upper airway

3.6.2 Comparison of aerodynamic parameters according to AN ratios

The AN ratios were calculated on lateral cephalograms applying the same measuring protocol in Study I [115]. An AN ratio of 0.6 was applied for dividing the cases into two subgroups: group 1: AN ratio < 0.6 and group 2: AN ratio ≥ 0.6 . The aerodynamic differences were compared between the subgroups in terms of the maximum velocity, the pressure drop, the maximum wall shear stress, and the minimum wall static pressure (**Figure 11**).

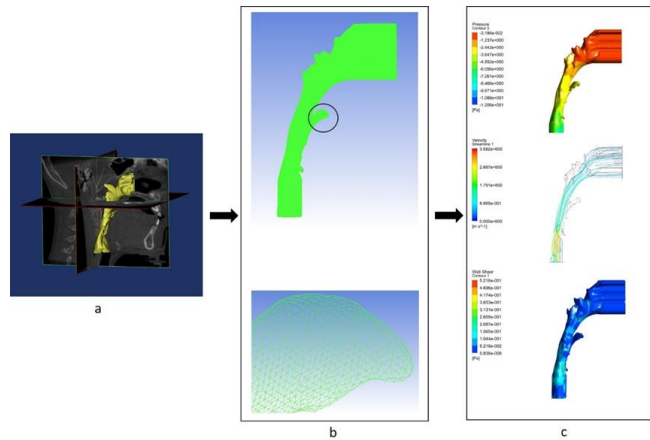


Figure 11. The procedure of CFD modeling and simulation. (a) CBCT segmentation; (b) Mesh generation and detailed zoom; (c) CFD simulation results: airflow pressure contour, velocity streamline, and wall shear stress contour.

Table 1 demonstrates the aerodynamic parameters in terms of the maximum velocity, the pressure drop, the maximum wall shear stress, and the minimum wall static pressure which were obtained from CFD simulation. Pressure drop refers to the pressure difference between a vertical plane through the most posterior point of the middle turbinate and a horizontal plane through the tip of the epiglottis.

Table 1. Description of the aerodynamic parameters evaluated applying the CFD simulation

Name	Unit	Definition
Maximum V_{ms}	m/s	The maximum velocity on the midsagittal plane
ΔP	Pa	The pressure loss of airflow between the defined two planes
Maximum P_{ws}	Pa	The maximum lateral pressure of airflow acting on the UA wall
Minimum P_w	Pa	The minimum vertical pressure of airflow acting on the UA wall

3.6.3 Comparison of the morphological and aerodynamic changes after RME

The seventeen subjects were divided into two groups based on the AN ratio at baseline (T0): group 1 comprised individuals with an AN ratio < 0.6 and group 2 with an AN ratio ≥ 0.6 .

Morphological assessment (Study III)

The UA was divided into the nasopharyngeal, retropalatal, and retroglossal airways by the reference planes in order to investigate the morphology of each region. After defining the axial planes at three inferior cross-sections – between the three airways and the UA – we were able to calculate the cross-sectional areas of the nasopharyngeal, retropalatal, and retroglossal spaces. The volumes of these spaces were automatically calculated after we had manually defined the boundaries. Morphological assessments including cross-sectional areas and volumes of each defined UA region are demonstrated in **Figure 12**.

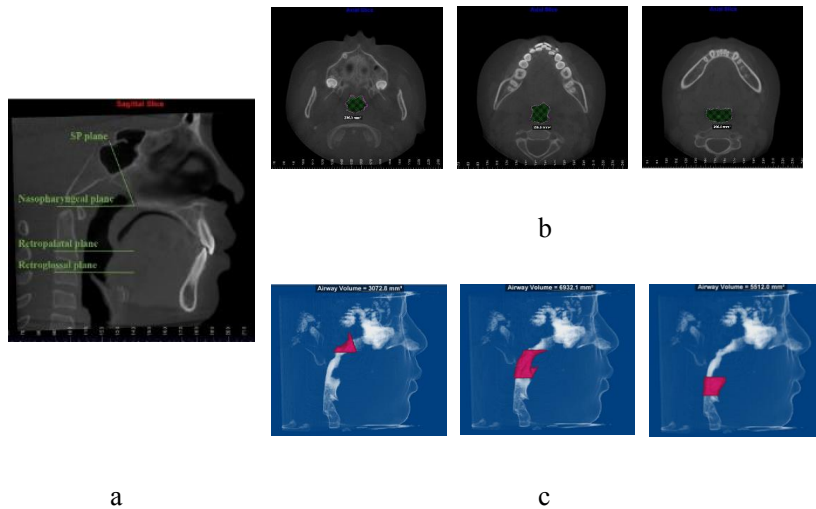


Figure 12. Morphological assessments of UA on CBCT images (a)The nasopharyngeal, retropalatal, and retroglottal upper airway was defined by four planes: the SP plane connects the midpoint of sella turcica and the posterior nasal spine, the nasopharyngeal, retropalatal, and retroglottal plane parallel to the horizontal plane passing through the point of posterior nasal, the tip of uvula, and the tip of the epiglottis respectively,(b) the cross-sectional areas, and (c) volumes were calculated for each region.

Aerodynamic assessment (Study IV)

Aerodynamic characteristics in terms of the maximum V_{ms} , ΔP , and maximum P_{ws} pre- and post-RME were simulated following the same process as Study II. To investigate the pressure drop of each region of UA, 4 planes were defined on the CFD model (**Figure 13**).

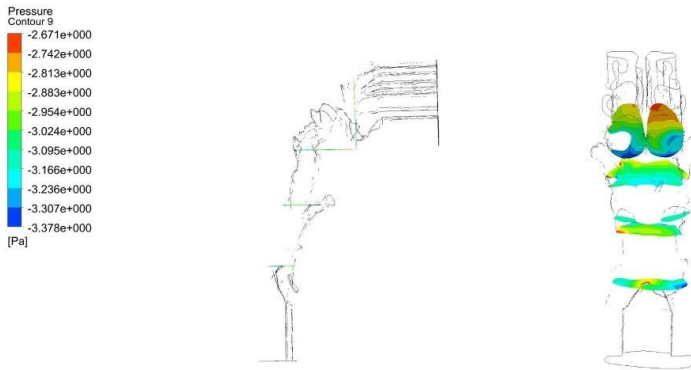


Figure 13. Description of the pressure of 4 planes defined on the CFD model. Definition of the four planes in the sagittal view: the superior plane, paralleled the inlet plane through the posterior point of middle turbinate; the following planes, paralleled the outlet plane through the inferior point of plane 1; the tip of the soft palate; the tip of the epiglottis respectively. The right graph shows the distribution of the pressure of each plane in the posterior view.

3.7 Statistical analyses

The statistical analyses were performed using IBM-SPSS version 25.0 (IBM, New York, NY, USA). Significance was set at *p-values* less than 0.05. Statistical tests for normality were conducted for all variables. Descriptive data for each group in Study III and Study IV were presented by applying Graph Pad Prism v 8.0 (GraphPad, USA).

Reliability

The Intraclass Correlation Coefficient (ICC) was applied for testing the intra- and inter-observer reliability (Study I–IV).

Association

The Association between the AN ratio and UA morphological parameters in terms of areas and volumes of nasopharyngeal and total upper airway were studied by scatter plots (Study I).

Comparison

The aerodynamic characteristics including ΔP , maximum V_{mx} , maximum P_{ws} , and minimum P_w in two groups divided by the AN ratio 0.6 were compared by independent samples t-test or Mann-Whitney U test (Study II). The paired samples t-test or Wilcoxon test was applied to compare the cross-sectional areas and volumes of nasopharyngeal, retropalatal, and retroglossal UA pre- and post-RME (Study III). The aerodynamic characteristics including ΔP , maximum V_{mx} , and maximum P_{ws} pre- and post-RME were compared by applying paired samples t-test or Wilcoxon test (Study IV).

Description

The morphological and aerodynamical differences between the two groups divided by AN ratios pre- and post-RME were expressed graphically in terms of mean and standard deviations (SD) (Study III and Study IV).

4. RESULTS

4.1 AN ratio Vs morphological characteristics (Study I)

Among the 55 cases, 32 were included in group A with a mean age and standard deviation of 11.8 ± 1.6 ; 23 were in group B with 21.1 ± 5.7 . The correlation coefficients between the AN ratio and nasopharyngeal volume were -0.78 and -0.57 for groups A (age ≤ 15 years) and B (age > 15 years), respectively (**Figure 14**). For repeated measurements of the AN ratio and nasopharyngeal volumes, ICC values ranged from 0.89 to 0.99 , within and between the two observers.

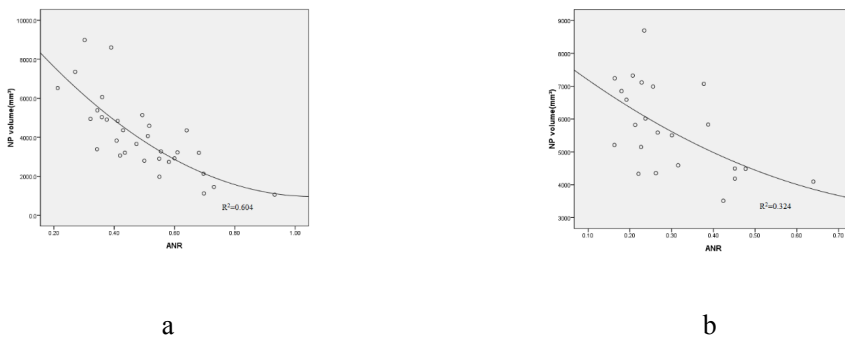


Figure 14. Scatter plots of the correlations between the AN ratio and nasopharyngeal volume: a - group A; b - group B

4.2 The aerodynamic characteristics according to AN ratios (Study II)

Study II involved thirty-five cases aged 12.0 ± 1.4 (13 females, 22 males). AN ratios ranged from 0.33 to 0.80 with a mean and standard deviation of 0.54 ± 0.15 . The maximum V_{ms} in Group 2 (AN ratio ≥ 0.6) exhibits a statistically significant increase of nearly 30% ($p < 0.05$) at both inspiration and expiration in contrast to Group 1 (AN ratio < 0.6). For the other aerodynamic parameters such as ΔP , maximum P_{ws} , and

minimum P_w , no significant difference was found between the two groups. The intra- and inter-observer reliability ranged between 0.872 and 0.997 for all measurements.

Figure 15 illustrates the airflow features in terms of velocity, wall static pressure, wall shear stress in two typical cases with an AN ratio of 0.40 and 0.73, respectively. The velocity streamlines in Figure 15a mainly composite mainly the lower velocity expressed by blue and green streamlines compared with the higher velocity expressed by green and yellow streamlines in Figure 15b.

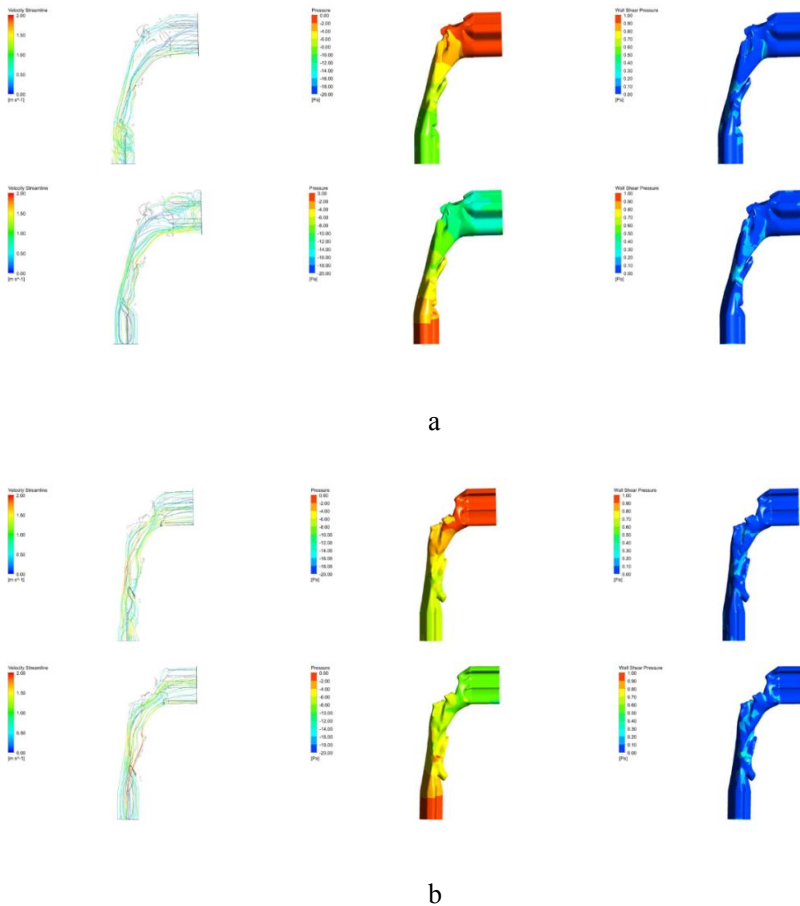


Figure 15. Illustration of the airflow feature in two typical cases with an AN ratio of 0.40 (a) and 0.73 (b), during inspiration (the up images) and expiration (the down images), respectively.

4.3 UA morphological and aerodynamic changes after RME (Study III, Study IV)

Seventeen cases with a mean age of 12.2 ± 1.3 years (6 females, 11 males) were eligible for inclusion in the study. The expansion was considered completed when the occlusal aspect of the maxillary lingual cusps of the upper first molars contacted the occlusal aspect of the vestibular cusp of the mandibular first molars. After achieving the desired expansion, the expander remained in place for 5.2 ± 1.7 months to stabilise the expansion. All the cases were divided into two groups at baseline (T0) with respect to AN ratios. Group 1 was comprised of 10 individuals (mean age 11.9 ± 1.3 years) with an AN ratio < 0.6 and group 2 encompassing 7 individuals (mean age 12.6 ± 1.3 years) with an AN ratio ≥ 0.6 . Due to the limited number of cases, group 1 and group 2 were merged when performing the statistical analysis on the effect of RME.

The UA morphology in terms of the nasopharyngeal, retropalatal, and retroglossal areas and volumes tended to increase after RME. The increasing percentage of the nasopharyngeal volume was most pronounced by 18.66%, but without statistical significance (**Table 2**). The morphological changes of each part of the airway were compared in terms of areas and volumes between the two groups at T0 and T1 (**Figure 16**).

Table 2. Airway area and volume measurements on cone beam computed tomography images before (T0) and after (T1) rapid maxillary expansion, and the change [(T1-T0)/T0%] in area and volume parameters during the treatment period (n = 17)

	T0		T1		Change (%)		p-value
	Mean	SD	Mean	SD	Mean	SD	
Area (mm²)							
Nasopharyngeal	320.16	113.10	319.31	115.78	2.82	34.93	0.965
Retropalatal	193.54	82.91	209.55	89.96	13.25	33.62	0.246
Retroglossal	237.96	95.74	241.25	107.32	3.18	27.20	0.776
Volume (mm³)							
Nasopharyngeal	3383.24	1648.17	3769.95	1670.48	18.66	43.83	0.246
Retropalatal	5450.11	1534.19	5781.52	2188.29	4.92	23.29	0.283
Retroglossal	4497.22	2488.35	4590.56	2161.19	8.22	30.35	0.619

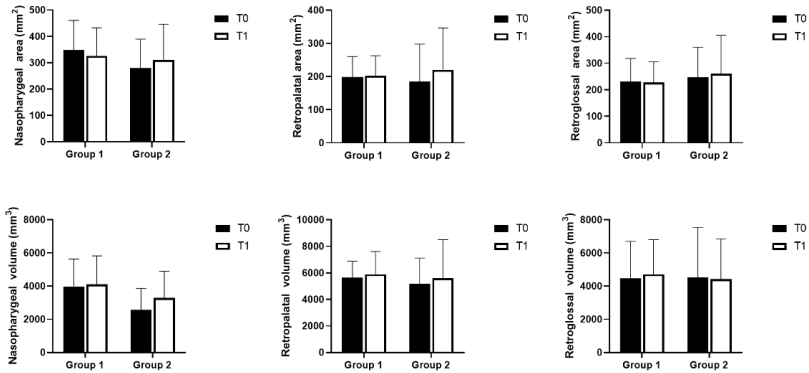


Figure 16. Morphological comparisons of nasopharyngeal, retropalatal and retroglottal airway in terms of areas and volumes (mean \pm SD) between the two groups at T0 and T1.

Regarding the aerodynamic changes after RME, except for ΔP at inspiration, all the other aerodynamic parameters decrease after RME treatment (**Table 3**). However, none of the changes was statistically significant. Nevertheless, V_{ms} (m/s) drop (2.79 to 2.28) at expiration being close to significance ($p = 0.057$).

Figure 17 illustrates the distributions of the aerodynamic variables for the two groups at T0 and T1 graphically. It demonstrates that group 2 has a higher mean ΔP and mean V_{ms} than group 1 at both inspiration and expiration regardless of T0 or T1, whereas the maximum P_{ws} shows the opposite trend being lower for group 2.

Table 3. Comparison of pressure drop (ΔP), maximum midsagittal velocity (V_{ms}), and maximum wall shear stress (P_{ws}) at inspiration and expiration before (T0) and after (T1) rapid maxillary expansion (n = 17).

	T0		T1		T0 Vs T1
	Mean	SD	Mean	SD	<i>p</i> -value
Inspiration					
ΔP (Pa)	-4.00	1.87	-4.36	2.45	0.549
Maximum V_{ms} (m/s)	2.48	0.70	2.43	0.92	0.906
Maximum P_{ws} (Pa)	1.29	1.24	1.03	1.32	0.163
Expiration					
ΔP (Pa)	2.96	2.56	2.81	2.43	0.943
Maximum V_{ms} (m/s)	2.79	1.09	2.28	0.82	0.057
Maximum P_{ws} (Pa)	1.63	1.85	0.93	0.71	0.381

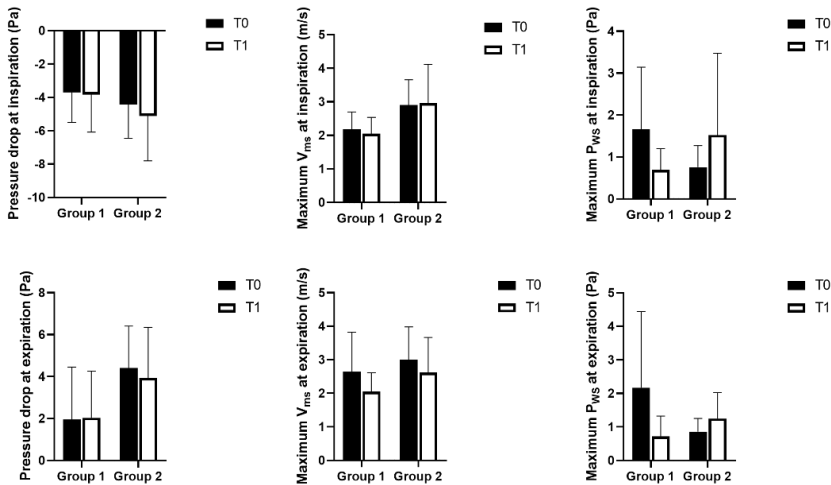


Figure 17. Expression of the aerodynamic characteristics in terms of mean, SD for the two groups at T0 and T1.

5. DISCUSSION

5.1 Methodology consideration

Due to the close association between adenoid size and maxillofacial development /obstructive breathing, orthodontists have suggested assessing the adenoid size prior to the start of treatment [34] [38]. Hence, an appropriate radiological modality for investigating adenoids is essential in the clinic. Lateral cephalogram is one of the most widely used images as an adjunct to clinical investigations of adenoid size. Although some studies have questioned its usefulness for AH diagnosis, without a doubt, it is the first choice of radiologic modalities for assessing adenoids with consideration of efficacy and rationality in the field of dentistry.

In the four retrospective studies, the lateral cephalograms and CBCT scans were already available according to various indications before orthodontic treatment. We utilised the readily available CBCT images and applied CFD simulation to detect the airflow characteristics. This keeps in line with the statement from the American Association of Orthodontists, which states that “The airway and surrounding structures, specifically the adenoids in children, should be evaluated, if radiographic records are taken for orthodontic purposes” [38]. Both approaches were considered as accurate and reliable methods for investigating UA, but neither CBCT nor CFD is a routine examination for orthodontic patients. Moreover, we must keep in mind that the CBCT scans have higher radiation doses than lateral cephalograms [116]. As CBCT scans only can be applied with a justified orthodontic indication, the investigation of UA by means of CBCT images and CFD simulation must remain a secondary assessment when the image was acquired for orthodontic diagnosis.

5.2 Interpretation of major findings

5.2.1 Lateral cephalogram Vs CBCT

2D Radiographs of the nasopharynx are sometimes misinterpreted because of the suboptimal imaging quality or the superimposition of the anatomic structures. It is well accepted that 3D imaging presents the UA's anatomic characters more effectively and accurately compared with 2D imaging. However, the CBCT scans are not the radiologic examination routinely performed on most orthodontic patients; meanwhile, the lateral cephalograms are more available during orthodontic process. Lateral cephalograms are most commonly applied in children and adolescents to depict and trace the skeletal structures and occlusion during the orthodontic treatment process. However, linear measurement showed lower method error compared with area and volume measurements [93], implying that a straightforward linear measurement may avoid bias from different software programs and the UA segmentation process.

Some researchers have searched for the parameters on 2D images to predict the UA morphology, such as the narrowest palate airway, the anterior airway width, the anatomic boundaries of the nasopharynx, and the AN ratio, which has been tested and correlated to nasopharyngeal volume. However, there is no consensus concerning an appropriate 2D parameter on the lateral cephalogram that could be used to estimate the 3D characteristics of the UA.

In Study I, the AN ratios measured on the lateral cephalograms were associated with volumes of nasopharynx and total UA in orthodontic patients. AN ratio was calculated by two linear measurements presenting the two main features of both the adenoid and nasopharynx. Therefore, the AN ratio seemed to be more rational for demonstrating the patency of the UA by assessing the relationship between adenoid and nasopharynx compare with the sole adenoidal or nasopharyngeal size.

During the measuring process of AN ratio, the most difficult part was to identify the fixed point of sphenobasioccipital synchondrosis for measuring N. Soldatova et al. [87] modified the AN ratio by using a perpendicular distance instead of

sphenobasioccipital synchondrosis. Fujioka et al. suggested that when sphenobasioccipital synchondrosis was not clearly visualised, it could be replaced by the site of crossing posteroinferior margin of lateral pterygoid plates and floor of bony nasopharynx [9]. Nevertheless, our results verified the classical AN ratio [9] to be a feasible measurement with high repeatability between and within examiners (0.89-0.96).

For patients 15 years or younger, the mean AN ratio was 0.49 and 0.54 in Study I and Study II, respectively, while the mean value was 0.30 in patients older than 15 years. The age-dependent distribution of AN ratio in our studies is coincident with the adenoidal physical development. The AN ratio gradually decreases from 0.52 at around 12 years and then sharply diminishes to 0.38 at around 15 years. After that, the adenoid size usually remains stable over the lifespan [9]. This may indicate that adenoidal size is a key factor for nasal obstruction in younger patients, but the effect may be weakened as the adenoids atrophy after 15 years. Furthermore, it may imply the different anatomic predisposing factors of SDB between children and adults. It has been well demonstrated that enlarged adenoid and/or palatal tonsils may lead to reduced patency in UA, which is the most common cause of developing SDB in children [117-119]. However, more complicated factors related to obstructed UA size results in SDB in adults, such as the abnormality of the cranial base, face height, maxilla, and mandible, or the increased size of the tongue and soft palate [120].

The AN ratio in group A (≤ 15 years) showed a higher correlation $r = -0.78$ with nasopharyngeal volume compared to $r = -0.57$ in group B (> 15 years). The correlation between AN ratio and nasopharyngeal volume is higher than the other linear measurements on lateral cephalograms. Sears et al. [101] reported that the distance through the midpoint of the nasopharynx showed the correlation $r = 0.43$ with nasopharyngeal volume. The nasopharyngeal area measured on lateral cephalogram has been reported to have a correlation of 0.45 with the nasopharyngeal volume [121]. A correlation of 0.75 has been found between the nasopharyngeal area and volume in the group of patients with a mean age of 14 years [102]. Compared to complicated area measurements of lateral cephalograms, we recommend the AN ratio for estimating the

nasopharyngeal volume. With respect to the total UA volume, the AN ratio also showed a correlation of $r = -0.48$ in younger patients. These results may contribute to the fact that for patients ≤ 15 years, a high AN ratio demonstrates a small nasopharyngeal and total UA volume.

The AN ratio measured on lateral cephalograms may be applied as a feasible 2D parameter by dentists for screening the nasopharyngeal morphology. However, in Study I, we solely provide morphological evidence without further functional evaluation i.e. airflow characteristics. Since a volumetric change in UA does not necessarily induce functional alteration, AN ratios should be associated with airflow features.

5.2.2 Lateral cephalogram Vs CFD simulation

To our knowledge, the AN ratio is first associated with UA's aerodynamic characteristics in this dissertation. Based on our results, the aerodynamic characteristics of the maximum V_{ms} significantly increased at both inspiration and expiration for patients with an AN ratio of more than 0.6. The finding demonstrated that an AN ratio of more than 0.6 induced airflow changes in terms of increased maximum V_{ms} . The velocity seemed to be one of the most sensitive aerodynamic parameters for representing the airflow alteration caused by UA morphological changes [51, 122]. Hu et al. [51] reported that a smaller coronal-sectional area indicated higher velocity on OSA patients without the other notable changes in aerodynamic characteristics. The relationship between UA morphology and airflow features can be explained by the Bernoulli's effect (**Figure 18**). Within a varying diameters tube, the narrower region forces fluid to gain a higher velocity and lower pressure [123].

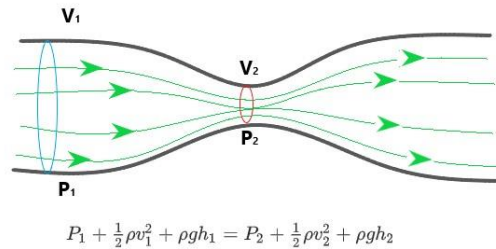


Figure 18. Bernoulli's principle.

The UA is a more complex structure in contrast to a smooth tube. The movements of surrounding soft tissue during respiration or the positional changes may influence the geometry of UA. In comparison with a soft palate and tongue, the adenoid located on the posterior part of the nasopharynx is less affected by the muscle tone, tongue position and neck flexion [124]. Mahboubi et al. [79] compared AN ratios measured on supine and erect positional lateral cephalograms and showed nearly the same AN ratios. As the adenoid is the most notable soft tissue located on the nasopharynx, the morphology of the nasopharynx is much more stable compared to the oropharynx [125] [126]. For patients ≤ 15 years, the AN ratio is a relatively stable parameter for estimating the nasopharyngeal volume and moreover, for predicting the UA aerodynamic features.

The AN ratio measured on the lateral cephalogram successfully represented the narrowing region leading to airflow aerodynamic alteration. It is possible, as a dentist, to target patients at risk of AH by AN ratios combined with clinical symptoms and possible complaints from patients or parents. Few studies addressed the threshold for identifying AH, and no standard was achieved. The AN ratio of 0.65 has been suggested for diagnosing a moderate nasopharyngeal obstruction [87]; an AN ratio of

0.73 [84] and the cross-sectional area $\leq 50 \text{ mm}^2$ measured on CT images [114] may imply an adenoidectomy. In our study, an AN ratio of more than 0.6 indicated a significant increase in the maximum V_{ms} , which revealed the aerodynamic changes caused by AH.

Previous CFD simulations were mostly conducted only at one respiratory phase, mostly the inspiration [51, 122, 127]. Since various aerodynamic parameters had been reported to be sensitive for expressing the airflow's feature at inspiration and expiration [128-130], in our CFD simulations, two respiratory phases were simulated, and the variation of aerodynamic characteristics at different respiratory phases revealed that both inspiration and expiration should be simulated.

The AN ratio exhibited high consistency with 3D morphology of UA in terms of nasopharyngeal volume; moreover, an AN ratio of more than 0.6 may imply the altered aerodynamic characteristics i.e. the maximum V_{ms} . The AN ratio can be used as a feasible tool for estimating AH by providing both morphological and aerodynamic evidence.

5.2.3 CBCT Vs CFD simulation

CBCT images make the complex anatomic structure within UA visible. The morphological parameters such as area and volume could be obtained from UA's segmentation on CBCT images. In the present study, CFD simulations were constructed based on CBCT images aiming to determine the association between morphology and aerodynamics.

With growing interest in the possible effect of RME on increasing UA space, many studies tried to assess the UA morphological changes after RME using CBCT images, but still without consistency [131-135]. The effect of RME on aerodynamics has been investigated sparsely. More evidence is warranted for determining the potential benefit for UA after RME.

In the engineering field, the pressure drop is defined as the pressure difference between two points of a fluid carrying network, which occurs when frictional forces,

caused by the resistance to flow, interact with fluid as it flows through the tube. Applying this concept to airflow passing through the UA, the pressure drops when facing physical force caused by morphological changes. Furthermore, the maximum V_{ms} may be altered following UA morphological changes. Faramarzi et al. evaluated the aerodynamics of the nasal cavity in a patient with septal perforation and found higher velocity at areas with higher pressure drop [136]. Regarding wall shear stress, it expresses the force per unit area exerted by the wall on the fluid in a direction on the local tangent plane [137]. The maximum P_{ws} locates primarily at the most constricted area [138]. A successful expansion of maxilla suture would hypothetically increase the UA's area and volume, resulting in declines in ΔP , maximum V_{ms} , and maximum P_{ws} .

In Study III and Study IV, the same group of patients who underwent RME treatment was assessed by means of the CBCT and CFD approaches, respectively. There was an overall tendency of enlarged UA's space, and most of the aerodynamic characteristics decreased accordingly after RME. However, neither morphological nor aerodynamic changes were statistically significant. In contrast to the present study, Iwasaki et al. found significant changes in aerodynamic characteristics in the nasal cavity after RME [139]. This may imply that the RME mainly increases the maxilla width in the transverse direction and the skeletal boundary of the nasal cavity was directly extended following the expanded maxilla [109].

Zhao et al. [113] reported that the morphological changes did not significantly correlate with the clinical response of mandibular advancement splints; in contrast, the aerodynamic changes were highly correlated with treatment outcome, suggesting that CFD simulation might be a more sensitive approach than 3D imaging in treatment outcome evaluation. However, we could not verify the superiority of aerodynamic changes over morphological changes in assessing the effect of RME treatment.

When the 17 cases were classified into two groups according to AN ratios, group 2 exhibited a more obvious decrease in nasopharyngeal volume compared with group 1 after RME. Regarding the aerodynamic changes, an opposite trend in maximum P_{ws} was observed between the two groups after RME. We speculate that the alteration of maximum P_{ws} may be caused by a weakened "adenoid jet" after RME. However, due

to limited cases and the diverse airflow characteristics in group 2, the random effect can not be excluded. Due to the small sample size, we did not perform statistical analysis on the effect of RME for the subgroup. Therefore, further study with more cases with severely enlarged adenoids is needed to confirm our assumption and target patients who may benefit from the RME.

CFD simulation provided aerodynamic data to better understand the UA's ventilation. At present, the simulation procedure is not entirely automatic and thus time-consuming. Part of the 3D segmentation and mesh generation needs to be performed manually due to the irregular anatomic structure of the UA. This may be the cause for the limited number of samples in the available CFD studies [111, 140, 141].

5.3 Clinical implication

As the AH may lead to maxillofacial dysmorphisms, pediatric OSA, behavioural and psychiatric problems, early detection of AH may help proper management and avoid further complications. Since children or their guardians may ignore the related obstructive symptoms, dentists are at the front line for targeting the patients at risk of AH among orthodontic patients.

Introducing a simple measure for dentists to estimate the UA and determining whether to refer the patients to ENT assessment is the most important purpose of this dissertation. Study I and Study II provide the morphological and aerodynamic evidence supporting the conclusion that an AN ratio could be applied as an efficient measuring parameter. The higher AN ratio, the higher risk of nasal congestion. Children who suffer from nasal congestion tend to alter their breathing habits to mouth breathing in order to overcome the nasal obstruction. Moreover, abnormal dental maxillofacial morphology related to obstructive breathing may be recognised by orthodontists. Consequently, an individual treatment plan including skeletal modification, muscle practice, and breathing training may be necessary.

AH is a common cause of nasal obstruction in children and adolescents. Knowledge of UA condition in this group of patients would help understand disease mechanism, assist diagnostics and evaluate treatment outcomes. The effect of RME on UA in terms of morphological and aerodynamic change could not be significantly verified in Study III and Study IV, indicating that the RME treatment could not reduce nasal obstruction caused by AH. The limited number of cases in Study III and Study IV might have also contributed to the absent effect of RME on UA.

6. CONCLUSIONS

1. The AN ratio is a simple 2D measuring parameter for estimating nasopharyngeal volumes of patients ≤ 15 years.
2. An AN ratio of more than 0.6 may predict the noticeably increased maximum V_{ms} , which could help orthodontists assess the UA's ventilation.
3. The maximum V_{ms} obtained from CFD simulation is the most sensitive parameter for representing aerodynamic characteristics of UA.
4. The effect of RME on UA in terms of morphology and aerodynamics are not significantly demonstrated by means of CBCT assessment and CFD simulation, respectively.
5. The aerodynamic characteristics in patients with AN ratio ≥ 0.6 may indicate a complicated airflow's alteration after RME treatment.

7. FUTURE PERSPECTIVES

Lateral cephalogram is the most commonly performed radiographic examination among orthodontic patients. Except for depicting and tracing occlusion, skeletal and soft structures during the orthodontic treatment process, the perspective of other pathological signs may reveal the risk associated with individual health, such as the patency of UA. Measurements of AN ratios shall, therefore, be implemented in the routine radiographic report. Further clinical studies are warranted to investigate the association between UA morphology, respiratory function, and clinical symptoms to better manage children with AH.

CFD simulation seems to be a promising method for assessing treatment effect in terms of aerodynamic characteristics, which has been confirmed by a number of studies on UA's ventilation after orthodontic, orthognathic and OSA-related oral appliance treatment [108, 122, 142]. This dissertation may further pave the way for applying this innovative approach to dental clinics in the future. By CFD simulation, we could discover the difference in aerodynamic characteristics in the UA when evaluating various treatments between responders and non-responders and help predict and improve the treatment outcome.

3D volumetric data and CFD simulation open the possibility of virtual therapeutic planning, such as virtual adenoidectomy. The desirable treatment outcome in anatomical and aerodynamic characteristics could be simulated on an individual-based 3D model at the treatment planning stage. We do believe, with the help of artificial intelligence, the CFD simulation procedure could be simplified and less time-consuming in the near future.

ACKNOWLEDGEMENTS

First, I would like to express my sincere gratitude to the Department of Clinical Dentistry, Faculty of Medicine, University of Bergen, for providing me the opportunity to carry out the doctoral education.

I am deeply grateful to my supervisors: Xie-Qi Shi, thank you for your guidance, encouragement, and unwavering support and belief in me during every single step of my Ph.D. journey; Kristina Hellén-Halme, I am indebted for your insightful comments and suggestions, your positivity and encouragement brightened my days and Stein Alte Lie, thank you for your valuable advice and patience, and your excellent statistical guidance throughout this Ph.D. project. I could not reach the destination without all your great support.

I am indebted to my supervisor of my master's thesis: Ailian Liu, for inspiring me to start my scientific career. I owe special thanks to Professor Gang Li, I sincerely appreciate your trust and valuable advice.

I would also like to extend my sincere thanks to my collaborators in China, Professor Weihua Cai, thank you for your imperative teaching in the CFD simulation and for hosting me during my stay at the Harbin Institute of Technology; Yicheng Chen, thank you for answering my never-ending questions concerning fluid dynamics, your optimism in the face of difficulties have made a deep impression.

To my colleagues in Sweden, Durer Iskanderani, Josefine Cederhag, and Randi Lynds, thank you for sharing your valuable learning experiences, your friendly and smiling faces have made our digital meeting enjoyable.

I am grateful to all my colleagues working on the 4th floor at IKO, thank you for sharing your scientific and personal experiences, your constant hard work and positivity encouraged me to keep going. Special thanks to Siren Østold, thank you for being so nice and your sweet good morning smile; to Kamal Mustafa and Cecilie Gjerde, thank you for including me in a great project; to my office mate Sid, I always

remind myself to be as energetic as you. Thank you for all your kind help and encouragement. It has been a privilege working with all of you!

Thanks to June Vibecke Knudtsen Indrevik, Elina Troscenko, and Connie Villemo Nilsen, thank you for guiding me through these Ph.D. years. Andreas Nesje, Randi Hansen, Marit Stubdal, Ann Lisbeth Garnes and the rest of the staff in the administration, thank you for always being so kind and helpful.

I wish to express my thanks to the staff of the Department of oral radiology, thank you for creating a warm working environment and making me feel welcome. Special thanks to Stig and Inger Johanne for the enjoyable working experience with you.

My dear friend Ying, I warmly thank you for inspiring me in frustrating moments. Jianhua, I am grateful for your absolutely smart tips for both research and life.

Finally, many thanks to my lovely family, Fengyi and Jojo, you are the sunshine in my life, thank you for sharing the daily news of what happened in school and kindergarten. Hui, thank you for your tremendous support and love. My parents, thank you for your everlasting care, love, encouragement, and support. I am so proud of having you in my life.

Xin Feng

February 2021

References

1. Schneider, C.V., *Liber de Tertius quo Novi Catarrhorum meatus demonstrantur*. Wittenbergae, Germany: Sumptibus Haered. D. Tobiae Mevii, & Elerdi Schumacheri: Excudebat Michael Wendt. 1661.
2. Waldeyer, W.U., *Ueber den lymphatischen Apparat des Pharynx*. Deutsche medizinische Wochenschrift, 1884. **10**(20): p. 315.
3. Perry, M. and A. Whyte, *Immunology of the Tonsils*. Immunology today, 1998. **19**: p. 414-21.
4. Karchev, T., *Specialization of tonsils as analyzers of the human immune system*. Acta Otolaryngol Suppl, 1988. **454**: p. 23-7.
5. Nave, H., A. Gebert, and R. Pabst, *Morphology and immunology of the human palatine tonsil*. Anat Embryol (Berl), 2001. **204**(5): p. 367-73.
6. Yang, W., et al., *Peripheral blood immunological parameters of children with adenoid hypertrophy with otitis media with effusion: propensity score matching*. Eur Arch Otorhinolaryngol, 2019. **276**(11): p. 3073-3080.
7. Miramontes, H.P., et al., *Prevalence of microorganisms and immunoglobulins in children with tonsillar hypertrophy and adenoiditis*. Int Arch Otorhinolaryngol, 2014. **18**(3): p. 311-5.
8. Capitano, M.A. and J.A. Kirkpatrick, *Nasopharyngeal Lymphoid Tissue*. Radiology, 1970. **96**(2): p. 389-391.
9. Fujioka, M., L.W. Young, and B.R. Girdany, *Radiographic evaluation of adenoidal size in children: adenoidal-nasopharyngeal ratio*. AJR Am J Roentgenol, 1979. **133**(3): p. 401-4.
10. Wang, D.Y., et al., *Assessment of adenoid size in children by fiberoptic examination*. Clin Otolaryngol Allied Sci, 1997. **22**(2): p. 172-7.
11. Pagella, F., et al., *Adenoids and clinical symptoms: Epidemiology of a cohort of 795 pediatric patients*. Int J Pediatr Otorhinolaryngol, 2015. **79**(12): p. 2137-41.
12. Feres, M.F., et al., *Endoscopic evaluation of adenoids: reproducibility analysis of current methods*. Clin Exp Otorhinolaryngol, 2013. **6**(1): p. 36-40.
13. Bitar, M.A., et al., *How frequent is adenoid obstruction? Impact on the diagnostic approach*. Pediatr Int, 2009. **51**(4): p. 478-83.
14. Cassano, P., et al., *Adenoid tissue rhinopharyngeal obstruction grading based on fiberendoscopic findings: a novel approach to therapeutic management*. Int J Pediatr Otorhinolaryngol, 2003. **67**(12): p. 1303-9.
15. Isaac, A., et al., *Correlations between acoustic rhinometry, subjective symptoms, and endoscopic findings in symptomatic children with nasal obstruction*. JAMA Otolaryngol Head Neck Surg, 2015. **141**(6): p. 550-5.
16. Pereira, L., et al., *Prevalence of adenoid hypertrophy: A systematic review and meta-analysis*. Sleep Med Rev, 2018. **38**: p. 101-112.
17. Aydin, S., et al., *Prevalence of adenoid hypertrophy and nocturnal enuresis in primary school children in Istanbul, Turkey*. Int J Pediatr Otorhinolaryngol, 2008. **72**(5): p. 665-8.
18. Faden, H., et al., *The ubiquity of asymptomatic respiratory viral infections in the tonsils and adenoids of children and their impact on airway obstruction*. Int J Pediatr Otorhinolaryngol, 2016. **90**: p. 128-132.
19. Comar, M., et al., *HHV-6 infection of tonsils and adenoids in children with hypertrophy and upper airway recurrent infections*. Int J Pediatr Otorhinolaryngol, 2010. **74**(1): p. 47-9.
20. van Kempen, M.J., G.T. Rijkers, and P.B. Van Cauwenberge, *The immune response in adenoids and tonsils*. Int Arch Allergy Immunol, 2000. **122**(1): p. 8-19.
21. Sadeghi-Shabestari, M., Y. Jabbari Moghaddam, and H. Ghaharri, *Is there any correlation between allergy and adenotonsillar tissue hypertrophy?* Int J Pediatr Otorhinolaryngol, 2011. **75**(4): p. 589-91.
22. Evcimik, M.F., et al., *Adenoid hypertrophy in children with allergic disease and influenza factors*. Int J Pediatr Otorhinolaryngol, 2015. **79**(5): p. 694-7.
23. Lawson, L.I., et al., *Effects of adenoidectomy on the speech of children with potential velopharyngeal dysfunction*. J Speech Hear Disord, 1972. **37**(3): p. 390-402.

24. Bhat, V., et al., *Association of asymptomatic otitis media with effusion in patients with adenoid hypertrophy*. J Otol, 2019. **14**(3): p. 106-110.
25. Abd Alhady, R. and M. el Sharnoubi, *Tympanometric findings in patients with adenoid hyperplasia, chronic sinusitis and tonsillitis*. J Laryngol Otol, 1984. **98**(7): p. 671-6.
26. Ulualp, S.O., et al., *Increased adenoid mast cells in patients with otitis media with effusion*. Int J Pediatr Otorhinolaryngol, 1999. **49**(2): p. 107-14.
27. Drager, L.F., et al., *OSA, Short Sleep Duration, and Their Interactions With Sleepiness and Cardiometabolic Risk Factors in Adults: The ELSA-Brasil Study*. Chest, 2019. **155**(6): p. 1190-1198.
28. Banno, K. and M.H. Kryger, *Sleep apnea: clinical investigations in humans*. Sleep Med, 2007. **8**(4): p. 400-26.
29. Gibson, G.J., *Obstructive sleep apnoea syndrome: underestimated and undertreated*. Br Med Bull, 2004. **72**: p. 49-65.
30. Joosten, K.F., et al., *How do we recognize the child with OSAS?* Pediatr Pulmonol, 2017. **52**(2): p. 260-271.
31. Marcus, C.L., et al., *Diagnosis and management of childhood obstructive sleep apnea syndrome*. Pediatrics, 2012. **130**(3): p. 576-84.
32. Peltonmäki, T., *The effect of mode of breathing on craniofacial growth--revisited*. Eur J Orthod, 2007. **29**(5): p. 426-9.
33. Sheeba, A.J. and S.S. Bakshi, *Adenoid Facies*. Anesthesiology, 2018. **129**(2): p. 334.
34. Koca, C.F., T. Erdem, and T. Bayındır, *The effect of adenoid hypertrophy on maxillofacial development: an objective photographic analysis*. J Otolaryngol Head Neck Surg, 2016. **45**(1): p. 48.
35. Linder-Aronson, S., *Adenoids. Their effect on mode of breathing and nasal airflow and their relationship to characteristics of the facial skeleton and the dentition. A biometric, rhinomanometric and cephalometro-radiographic study on children with and without adenoids*. Acta Otolaryngol Suppl, 1970. **265**: p. 1-132.
36. Meyer, H., *Om adenoide Vegetationer Nasesvaelgrummet*. Hospitalstidende, 1868. **11**.
37. Huang, Y.S. and C. Guilleminault, *Pediatric obstructive sleep apnea and the critical role of oral-facial growth: evidences*. Front Neurol, 2012. **3**: p. 184.
38. Behrents, R.G., et al., *Obstructive sleep apnea and orthodontics: An American Association of Orthodontists White Paper*. Am J Orthod Dentofacial Orthop, 2019. **156**(1): p. 13-28.e1.
39. Ruben, R.J., *The adenoid: Its history and a cautionary tale*. The Laryngoscope, 2017. **127**(S2): p. S13-S28.
40. Parker, L.P., et al., *Rhinomanometry in children*. Int J Pediatr Otorhinolaryngol, 1989. **17**(2): p. 127-37.
41. Cho, J.H., et al., *Size assessment of adenoid and nasopharyngeal airway by acoustic rhinometry in children*. J Laryngol Otol, 1999. **113**(10): p. 899-905.
42. Marques, V.C. and W.T. Anselmo-Lima, *Pre- and postoperative evaluation by acoustic rhinometry of children submitted to adenoidectomy or adenotonsillectomy*. Int J Pediatr Otorhinolaryngol, 2004. **68**(3): p. 311-6.
43. Kindermann, C.A., R. Roithmann, and J.F. Lubianca Neto, *Sensitivity and specificity of nasal flexible fiberoptic endoscopy in the diagnosis of adenoid hypertrophy in children*. Int J Pediatr Otorhinolaryngol, 2008. **72**(1): p. 63-7.
44. Kubba, H. and B.J. Bingham, *Endoscopy in the assessment of children with nasal obstruction*. J Laryngol Otol, 2001. **115**(5): p. 380-4.
45. Pallanch, J., *Physiology: Rhinomanometry*, in *Nasal Physiology and Pathophysiology of Nasal Disorders*, T.M. Önerci, Editor. 2013, Springer Berlin Heidelberg: Berlin, Heidelberg. p. 331-344.
46. Bhatia, K.S.S., et al., *Nasopharyngeal Mucosa and Adenoids: Appearance at MR Imaging*. Radiology, 2012. **263**(2): p. 437-443.
47. Selvadurai, S., et al., *Utility of brain MRI in children with sleep-disordered breathing*. Laryngoscope, 2017. **127**(2): p. 513-519.
48. Farid, M. and N. Metwalli, *Computed tomographic evaluation of mouth breathers among paediatric patients*. Dentomaxillofac Radiol, 2010. **39**(1): p. 1-10.

49. Cohen, O., et al., *Development of the nasopharynx: A radiological study of children*. Clin Anat, 2020. **33**(7): p. 1019-1024.
50. Surov, A., et al., *Diffusion weighted imaging of nasopharyngeal adenoid hypertrophy*. Acta Radiol, 2015. **56**(5): p. 587-91.
51. Hu, C., et al., *Investigation of resectability degree for adenoidal surgery in OSA children with the method of computational fluid dynamics*. Acta Otolaryngol, 2017. **137**(1): p. 82-85.
52. Buskens, E., et al., *Adenotonsillectomy or watchful waiting in patients with mild to moderate symptoms of throat infections or adenotonsillar hypertrophy: a randomized comparison of costs and effects*. Arch Otolaryngol Head Neck Surg, 2007. **133**(11): p. 1083-8.
53. Egeli, E., et al., *Measuring the correlation between adenoidal-nasopharyngeal ratio (AN ratio) and tympanogram in children*. International Journal of Pediatric Otorhinolaryngology, 2005. **69**(2): p. 229-233.
54. Sakarya, E.U., et al., *Use of intranasal corticosteroids in adenotonsillar hypertrophy*. J Laryngol Otol, 2017. **131**(5): p. 384-390.
55. Sun, Y.L., et al., *Effectiveness and safety of Chinese herbal medicine for pediatric adenoid hypertrophy: A meta-analysis*. Int J Pediatr Otorhinolaryngol, 2019. **119**: p. 79-85.
56. Bhattacharyya, N. and H.W. Lin, *Changes and consistencies in the epidemiology of pediatric adenotonsillar surgery, 1996-2006*. Otolaryngol Head Neck Surg, 2010. **143**(5): p. 680-4.
57. Haapkyla, J., et al., *Trends in otitis media surgery: a decrease in adenoidectomy*. Int J Pediatr Otorhinolaryngol, 2008. **72**(8): p. 1207-13.
58. Gerhardsson, H., et al., *Pediatric adenoid surgery in Sweden 2004-2013: Incidence, indications and concomitant surgical procedures*. Int J Pediatr Otorhinolaryngol, 2016. **87**: p. 61-6.
59. Goldstein, N.A., et al., *Clinical assessment of pediatric obstructive sleep apnea*. Pediatrics, 2004. **114**(1): p. 33-43.
60. Chorney, S.R. and K.B. Zur, *Adenoidectomy Without Tonsillectomy for Pediatric Obstructive Sleep Apnea*. Otolaryngol Head Neck Surg, 2020: 0194599820955172.
61. Sanders, J.C., et al., *Perioperative complications of adenotonsillectomy in children with obstructive sleep apnea syndrome*. Anesth Analg, 2006. **103**(5): p. 1115-21.
62. Byars, S.G., S.C. Stearns, and J.J. Boomsma, *Association of Long-Term Risk of Respiratory, Allergic, and Infectious Diseases With Removal of Adenoids and Tonsils in Childhood*. JAMA Otolaryngol Head Neck Surg, 2018. **144**(7): p. 594-603.
63. Marcus, C.L., et al., *A randomized trial of adenotonsillectomy for childhood sleep apnea*. N Engl J Med, 2013. **368**(25): p. 2366-76.
64. Pawłowska-Seredyńska, K., et al., *Craniofacial proportions in children with adenoid or adenotonsillar hypertrophy are related to disease duration and nasopharyngeal obstruction*. Int J Pediatr Otorhinolaryngol, 2020. **132**: 109911.
65. Macari, A.T., M.A. Bitar, and J.G. Ghafari, *New insights on age-related association between nasopharyngeal airway clearance and facial morphology*. Orthod Craniofac Res, 2012. **15**(3): p. 188-97.
66. Guilleminault, C. and F. Akhtar, *Pediatric sleep-disordered breathing: New evidence on its development*. Sleep Medicine Reviews, 2015. **24**: p. 46-56.
67. Marchisio, P., et al., *Clinical assessment of adenoidal obstruction based on the nasal obstruction index is no longer useful in children*. Otolaryngol Head Neck Surg, 2010. **142**(2): p. 237-41.
68. McNamara, J.A., Jr., et al., *The role of rapid maxillary expansion in the promotion of oral and general health*. Prog Orthod, 2015. **16**: p. 33.
69. Handelman, C.S. and G. Osborne, *Growth of the nasopharynx and adenoid development from one to eighteen years*. Angle Orthod, 1976. **46**(3): p. 243-59.
70. Mlynarek, A., et al., *Lateral neck radiography versus direct video rhinoscopy in assessing adenoid size*. J Otolaryngol, 2004. **33**(6): p. 360-5.
71. Major, M.P., C. Flores-Mir, and P.W. Major, *Assessment of lateral cephalometric diagnosis of adenoid hypertrophy and posterior upper airway obstruction: a systematic review*. Am J Orthod Dentofacial Orthop, 2006. **130**(6): p. 700-8.

72. Kugelman, N., et al., *Adenoid Obstruction Assessment in Children: Clinical Evaluation Versus Endoscopy and Radiography*. Isr Med Assoc J, 2019. **21**(6): p. 376-380.
73. Kolo, E.S., et al., *Plain radiographic evaluation of children with obstructive adenoids*. Eur J Radiol, 2011. **79**(2): e38-41.
74. Ysunza, A., et al., *Video fluoroscopy for evaluating adenoid hypertrophy in children*. International Journal of Pediatric Otorhinolaryngology, 2008. **72**(8): p. 1159-1165.
75. Major, M.P., et al., *The accuracy of diagnostic tests for adenoid hypertrophy: A systematic review*. The Journal of the American Dental Association, 2014. **145**(3): p. 247-254.
76. Duan, H., et al., *Accuracy of lateral cephalogram for diagnosis of adenoid hypertrophy and posterior upper airway obstruction: A meta-analysis*. Int J Pediatr Otorhinolaryngol, 2019. **119**: p. 1-9.
77. Filho, D.I., et al., *A comparison of nasopharyngeal endoscopy and lateral cephalometric radiography in the diagnosis of nasopharyngeal airway obstruction*. Am J Orthod Dentofacial Orthop, 2001. **120**(4): p. 348-52.
78. Holmberg, H. and S. Linder-Aronson, *Cephalometric radiographs as a means of evaluating the capacity of the nasal and nasopharyngeal airway*. Am J Orthod, 1979. **76**(5): p. 479-90.
79. Mahboubi, S., et al., *The lateral neck radiograph in adenotonsillar hyperplasia*. Int J Pediatr Otorhinolaryngol, 1985. **10**(1): p. 67-73.
80. Kemaloglu, Y.K., et al., *Radiographic Evaluation of Children with Nasopharyngeal Obstruction Due to the Adenoid*. Annals of Otolaryngology, Rhinology & Laryngology, 1999. **108**(1): p. 67-72.
81. Pathak, K., N.R. Ankale, and A.S. Harugop, *Comparison Between Radiological Versus Endoscopic Assessment of Adenoid Tissue in Patients of Chronic Adenoiditis*. Indian J Otolaryngol Head Neck Surg, 2019. **71**(Suppl 1): p. 981-985.
82. Acar, M., et al., *Method of the diagnosis of adenoid hypertrophy for physicians: adenoid-nasopharynx ratio*. J Craniofac Surg, 2014. **25**(5): e438-40.
83. Talebian, S., et al., *Comparison of adenoid size in lateral radiographic, pathologic, and endoscopic measurements*. Electron Physician, 2018. **10**(6): p. 6935-6941.
84. Elwany, S., *The adenoidal-nasopharyngeal ratio (AN ratio). Its validity in selecting children for adenoidectomy*. J Laryngol Otol, 1987. **101**(6): p. 569-73.
85. Jeans, W.D., D.C. Fernando, and A.R. Maw, *How should adenoidal enlargement be measured? A radiological study based on interobserver agreement*. Clin Radiol, 1981. **32**(3): p. 337-40.
86. Caylakli, F., et al., *Correlation between adenoid-nasopharynx ratio and endoscopic examination of adenoid hypertrophy: a blind, prospective clinical study*. Int J Pediatr Otorhinolaryngol, 2009. **73**(11): p. 1532-5.
87. Soldatova, L., et al., *Lateral Neck Radiography in Preoperative Evaluation of Adenoid Hypertrophy*. Ann Otol Rhinol Laryngol, 2020. **129**(5): p. 482-488.
88. ICRP, 1977. *Recommendations of the ICRP*. ICRP Publication 26. Ann. ICRP 1 (3).
89. ICRP, 2015. *Radiological Protection in Cone Beam Computed Tomography (CBCT)*. ICRP Publication 129. Ann. ICRP 44(1).
90. Mozzo, P., et al., *A new volumetric CT machine for dental imaging based on the cone-beam technique: preliminary results*. Eur Radiol, 1998. **8**(9): p. 1558-64.
91. Ludlow, J.B. and M. Ivanovic, *Comparative dosimetry of dental CBCT devices and 64-slice CT for oral and maxillofacial radiology*. Oral Surg Oral Med Oral Pathol Oral Radiol Endod, 2008. **106**(1): p. 106-14.
92. El, H. and J.M. Palomo, *Measuring the airway in 3 dimensions: a reliability and accuracy study*. Am J Orthod Dentofacial Orthop, 2010. **137**(4 Suppl): S50.e1-9; discussion S50-2.
93. Di Carlo, G., et al., *A new simple three-dimensional method to characterize upper airway in orthognathic surgery patient*. Dentomaxillofac Radiol, 2017: 20170042.
94. Guijarro-Martinez, R. and G.R.J. Swennen, *Three-dimensional cone beam computed tomography definition of the anatomical subregions of the upper airway: a validation study*. International Journal of Oral and Maxillofacial Surgery, 2013. **42**(9): 1140-1149.
95. Chen, H., et al., *Accuracy of MDCT and CBCT in three-dimensional evaluation of the oropharynx morphology*. Eur J Orthod, 2018. **40**(1): 58-64.

96. Castro-Silva, L., et al., *Cone-beam evaluation of pharyngeal airway space in class I, II, and III patients*. Oral Surgery, Oral Medicine, Oral Pathology and Oral Radiology, 2015. **120**(6): p. 679-683.
97. Mordente, C.M., et al., *Upper airway assessment using four different maxillary expanders in cleft patients: A cone-beam computed tomography study*. Angle Orthod, 2016. **86**(4): p. 617-24.
98. Kumar.V, A., et al., *Pharyngeal Airway Dimension in Different Types of Malocclusion*. International Journal of Dental Sciences and Research, 2014. **2**(4A): p. 7-11.
99. Yoon, A., et al., *Distraction Osteogenesis Maxillary Expansion (DOME) for adult obstructive sleep apnea patients with narrow maxilla and nasal floor*. Sleep Med, 2020. **65**: p. 172-176.
100. Major, M.P., et al., *Agreement between cone-beam computed tomography and nasoendoscopy evaluations of adenoid hypertrophy*. American Journal of Orthodontics and Dentofacial Orthopedics, 2014. **146**(4): p. 451-459.
101. Sears, C.R., et al., *Comparison of pharyngeal airway changes on plain radiography and cone-beam computed tomography after orthognathic surgery*. J Oral Maxillofac Surg, 2011. **69**(11): e385-94.
102. Aboudara, C., et al., *Comparison of airway space with conventional lateral headfilms and 3-dimensional reconstruction from cone-beam computed tomography*. Am J Orthod Dentofacial Orthop, 2009. **135**(4): p. 468-79.
103. Shete, C.S. and W.A. Bhad, *Three-dimensional upper airway changes with mandibular advancement device in patients with obstructive sleep apnea*. American Journal of Orthodontics and Dentofacial Orthopedics, 2017. **151**(5): p. 941-948.
104. Pinheiro de Magalhaes Bertoz, A., et al., *Three-dimensional airway changes after adenotonsillectomy in children with obstructive apnea: Do expectations meet reality?* Am J Orthod Dentofacial Orthop, 2019. **155**(6): p. 791-800.
105. Feletti, A., et al., *Computational Fluid Dynamics Analysis and Correlation with Intraoperative Aneurysm Features*. Acta Neurochir Suppl, 2018. **129**: p. 3-9.
106. Hassan, T., et al., *A proposed parent vessel geometry-based categorization of saccular intracranial aneurysms: computational flow dynamics analysis of the risk factors for lesion rupture*. J Neurosurg, 2005. **103**(4): p. 662-80.
107. Murayama, Y., et al., *Computational fluid dynamics as a risk assessment tool for aneurysm rupture*. Neurosurg Focus, 2019. **47**(1):E12.
108. Kita, S., et al., *Computational Fluid Dynamic Study of Nasal Respiratory Function Before and After Bimaxillary Orthognathic Surgery With Bone Trimming at the Inferior Edge of the Pyriform Aperture*. J Oral Maxillofac Surg, 2016. **74**(11): p. 2241-2251.
109. Iwasaki, T., et al., *Improvement of nasal airway ventilation after rapid maxillary expansion evaluated with computational fluid dynamics*. Am J Orthod Dentofacial Orthop, 2012. **141**(3): p. 269-278.
110. Iwasaki, T., et al., *How does distraction osteogenesis maxillary expansion (DOME) reduce severity of obstructive sleep apnea?* Sleep Breath, 2020. **24**(1): p. 287-296.
111. Martínez, A., et al., *Physiological and geometrical effects in the upper airways with and without mandibular advance device for sleep apnea treatment*. Scientific reports, 2020. **10**(1): 5322.
112. Kim, T., et al., *Change in the Upper Airway of Patients With Obstructive Sleep Apnea Syndrome Using Computational Fluid Dynamics Analysis: Conventional Maxillomandibular Advancement Versus Modified Maxillomandibular Advancement With Anterior Segmental Setback Osteotomy*. J Craniofac Surg, 2015.**26**(8):e765-70.
113. Zhao, M., et al., *Computational fluid dynamics for the assessment of upper airway response to oral appliance treatment in obstructive sleep apnea*. Journal of Biomechanics, 2013. **46**(1): p. 142-150.
114. Iwasaki, T., et al., *Effect of adenoids and tonsil tissue on pediatric obstructive sleep apnea severity determined by computational fluid dynamics*. J Clin Sleep Med, 2020. **16**(12): p. 2021-2028.

-
115. Feng, X., et al., *Comparative analysis of upper airway volume with lateral cephalograms and cone-beam computed tomography*. Am J Orthod Dentofacial Orthop, 2015. **147**(2): p. 197-204.
 116. Kadesjö, N., et al., *Radiation dose from X-ray examinations of impacted canines: cone beam CT vs two-dimensional imaging*. Dentomaxillofac Radiol, 2018. **47**(3): 20170305.
 117. Arens, R. and C.L. Marcus, *Pathophysiology of upper airway obstruction: a developmental perspective*. Sleep, 2004. **27**(5): p. 997-1019.
 118. Redline, S., et al., *The Childhood Adenotonsillectomy Trial (CHAT): rationale, design, and challenges of a randomized controlled trial evaluating a standard surgical procedure in a pediatric population*. Sleep, 2011. **34**(11): p. 1509-17.
 119. Baik, G. and S.E. Brietzke, *Cost Benefit and Utility Decision Analysis of Turbinoplasty with Adenotonsillectomy for Pediatric Sleep-Disordered Breathing*. Otolaryngol Head Neck Surg, 2019. **161**(2): p. 343-347.
 120. Neelapu, B.C., et al., *Craniofacial and upper airway morphology in adult obstructive sleep apnea patients: A systematic review and meta-analysis of cephalometric studies*. Sleep Med Rev, 2017. **31**: p. 79-90.
 121. Aras, I., S. Olmez, and S. Dogan, *Comparative Evaluation of Nasopharyngeal Airways of Unilateral Cleft Lip and Palate Patients Using Three-Dimensional and Two-Dimensional Methods*. The Cleft Palate-Craniofacial Journal, 2012. **49**(6): p. 75-81.
 122. Iwasaki T Fau - Sato, H., et al., *Herbst appliance effects on pharyngeal airway ventilation evaluated using computational fluid dynamics*. Angle Orthod, 2017. **87**(3): p. 397-403.
 123. Weese, J., et al., *CFD- and Bernoulli-based pressure drop estimates: A comparison using patient anatomies from heart and aortic valve segmentation of CT images*. Med Phys, 2017. **44**(6): p. 2281-2292.
 124. Alsufyani, N.A., et al., *Cone beam computed tomography registration for 3-D airway analysis based on anatomic landmarks*. Oral Surgery, Oral Medicine, Oral Pathology and Oral Radiology, 2014. **118**(3): p. 371-383.
 125. Vizzotto, M.B., et al., *A comparative study of lateral cephalograms and cone-beam computed tomographic images in upper airway assessment*. Eur J Orthod, 2012. **34**(3): p. 390-3.
 126. Van Holsbeke, C.S., et al., *Change in upper airway geometry between upright and supine position during tidal nasal breathing*. J Aerosol Med Pulm Drug Deliv, 2014. **27**(1): p. 51-7.
 127. Lee, H.P., et al., *Changes of airflow pattern in inferior turbinate hypertrophy: a computational fluid dynamics model*. Am J Rhinol Allergy, 2009. **23**(2): p. 153-8.
 128. Wakayama, T., M. Suzuki, and T. Tanuma, *Effect of Nasal Obstruction on Continuous Positive Airway Pressure Treatment: Computational Fluid Dynamics Analyses*. PLoS One, 2016. **11**(3): e0150951.
 129. Iwasaki, T.A.-O.h.o.o., et al., *Influence of pharyngeal airway respiration pressure on Class II mandibular retrusion in children: A computational fluid dynamics study of inspiration and expiration*. Orthod Craniofac Res, 2017. **20**(2):95-101.
 130. Tan, J., et al., *Numerical simulation for the upper airway flow characteristics of Chinese patients with OSAHS using CFD models*. Eur Arch Otorhinolaryngol, 2013. **270**(3): p. 1035-43.
 131. Ribeiro, A.N., et al., *Upper airway expansion after rapid maxillary expansion evaluated with cone beam computed tomography*. Angle Orthod, 2012. **82**(3): p. 458-63.
 132. Zhao, Y., et al., *Oropharyngeal airway changes after rapid palatal expansion evaluated with cone-beam computed tomography*. Am J Orthod Dentofacial Orthop, 2010. **137**(4 Suppl): p. S71-8.
 133. Almuzian, M., et al., *Does rapid maxillary expansion affect nasopharyngeal airway? A prospective Cone Beam Computerised Tomography (CBCT) based study*. The Surgeon, 2018. **16**(1): p. 1-11.
 134. Smith, T., et al., *Three-dimensional computed tomography analysis of airway volume changes after rapid maxillary expansion*. Am J Orthod Dentofacial Orthop, 2012. **141**(5): p. 618-26.
 135. Kavand, G., et al., *Retrospective CBCT analysis of airway volume changes after bone-borne vs tooth-borne rapid maxillary expansion*. Angle Orthod, 2019. **89**(4): p. 566-574.

136. Faramarzi, M., et al., *Numerical investigation of the flow field in realistic nasal septal perforation geometry*. Allergy Rhinol (Providence), 2014. **5**(2): p. 70-7.
137. Katritsis, D., et al., *Wall shear stress: theoretical considerations and methods of measurement*. Prog Cardiovasc Dis, 2007. **49**(5): p. 307-29.
138. Murata, N., et al., *High shear stress on the coronary arterial wall is related to computed tomography-derived high-risk plaque: a three-dimensional computed tomography and color-coded tissue-characterizing intravascular ultrasonography study*. Heart Vessels, 2019. **34**(9): p. 1429-1439.
139. Iwasaki, T., et al., *The effect of rapid maxillary expansion on pharyngeal airway pressure during inspiration evaluated using computational fluid dynamics*. Int J Pediatr Otorhinolaryngol, 2014. **78**(8): p. 1258-64.
140. Lambeth, C., et al., *Modelling mucosal surface roughness in the human velopharynx: a computational fluid dynamics study of healthy and obstructive sleep apnea airways*. J Appl Physiol (1985), 2018.
141. Mortazavy Beni, H., K. Hassani, and S. Khorrasmeh, *In silico investigation of sneezing in a full real human upper airway using computational fluid dynamics method*. Comput Methods Programs Biomed, 2019. **177**: p. 203-209.
142. Chen, H., et al., *Analyses of aerodynamic characteristics of the oropharynx applying CBCT: obstructive sleep apnea patients versus control subjects*. Dentomaxillofac Radiol, 2018. **47**(2): 20170238.

Original Papers

Comparative analysis of upper airway volume with lateral cephalograms and cone-beam computed tomography

Xin Feng, Gang Li, Zhenyu Qu, Lin Liu, Karin N Näsström, Xie-Qi Shi.

American Journal of Orthodontics and Dentofacial Orthopedics, 2015. 147(2): p. 197-204. doi:
10.1016/j.ajodo. 2014.10.025

Comparative analysis of upper airway volume with lateral cephalograms and cone-beam computed tomography

Xin Feng,^a Gang Li,^b Zhenyu Qu,^c Lin Liu,^d Karin Näsström,^e and Xie-Qi Shi^f

Dalian and Beijing, China, and Huddinge, Sweden

Introduction: In this study, we aimed to evaluate the adenoidal nasopharyngeal ratio (ANR) on lateral cephalograms by assessing upper airway volumes using cone-beam computed tomography (CBCT) images as the validation method. **Methods:** Fifty-five patients were included in the study, and it was essential that the lateral cephalograms and CBCT images taken at their examinations were not more than 1 week apart. There were 32 subjects in group A (age ≤ 15 years) and 23 subjects in group B (age > 15 years). The ANR was measured on the lateral cephalograms. The area and volumetric measurements of the nasopharynx and the total upper airway were obtained from CBCT images. Repeated measurements of the ANR and airway volume were performed on 10 subjects by 2 observers. **Results:** Group A had a higher correlation ($r = -0.78$) between the ANR and the nasopharynx volume than did group B ($r = -0.57$). The ANR had a weak correlation with the total upper airway volume (group A, $r = -0.48$; group B, $r = -0.32$). Both measurements made on lateral cephalograms and CBCT were highly reproducible in terms of intraobserver and interobserver agreement. **Conclusions:** Based on our results, the measurement of the ANR on lateral cephalograms can be used as an initial screening method to estimate the nasopharynx volumes of younger patients (age ≤ 15 years). (Am J Orthod Dentofacial Orthop 2015;147:197-204)

Obstruction of the airway often alters normal breathing, which has a significant impact on the development of craniofacial structures,^{1,2} such as incompetent lips, lower or anterior tongue position, narrow maxillary arch, long face height, crossbites, and posteroinferior rotation of the mandible.³ The most common reason for obstruction of the airway is adenoid hypertrophy. Adenoids are a collection of lymphoid tissues in the posterior nasopharyngeal wall; they are small at

birth but progressively enlarge as a result of increased immunologic activity.⁴ Repeated adenoidal infection and inflammation or genetic factors may lead to pharyngeal obstruction, causing mouth breathing, which can in turn result in altered craniofacial development.⁵

Before planning orthodontic treatment, orthodontists should view and analyze the airway region on a lateral cephalogram. If an obstruction is observed, the patient might be referred to an otolaryngologist for further treatment. A diagnostic method that can accurately provide data on the severity of nasopharyngeal obstruction is important for both dentists and medical specialists. Several methods may be used for evaluating the size of adenoidal tissues, including conventional lateral cephalogram, nasal endoscopy, acoustic rhinometry, rhinomanometry, computed tomography, and magnetic resonance imaging. Among these methods, the conventional lateral cephalogram was reported to be the most cost effective, reproducible, and easy to interpret in assessing the size of adenoidal tissues.⁶⁻⁸ A lateral cephalogram is useful for analyzing adenoidal tissues and the nasopharyngeal airway; however, it is a 2-dimensional imaging modality that has limitations to represent 3-dimensional (3D) structures. Several studies have reported that computed tomography and magnetic resonance imaging may provide more clinically useful

^aRadiologist, Department of Oral and Maxillofacial Radiology, Stomatological Hospital, Dalian, China; guest researcher, Oral Maxillofacial Diagnostics and Surgery, Karolinska Institutet, Huddinge, Sweden.

^bProfessor, Department of Oral and Maxillofacial Radiology, School and Hospital of Stomatology, Peking University, Beijing, China.

^cAssociate professor, Department of Oral and Maxillofacial Radiology, Stomatological Hospital, Dalian, China.

^dProfessor, Department of Orthodontics, Stomatological Hospital, Dalian, China.

^eChair, Oral Maxillofacial Diagnostics and Surgery, Karolinska Institutet, Huddinge, Sweden.

^fAssociate professor, Oral Maxillofacial Diagnostics and Surgery, Karolinska Institutet, Huddinge, Sweden.

All authors have completed and submitted the ICMJE Form for Disclosure of Potential Conflicts of Interest, and none were reported.

Address correspondence to: Xie-Qi Shi, Department of Dental Medicine, Box 4064, 14104 Huddinge, Sweden; e-mail, Xie.Qi.Shi@ki.se.

Submitted, January 2014; revised and accepted, October 2014.

0889-5406/\$36.00

Copyright © 2015 by the American Association of Orthodontists.

<http://dx.doi.org/10.1016/j.ajodo.2014.10.025>

data to supplement the information from the 2-dimensional images.^{9,10} Recently, with the introduction of cone-beam computed tomography (CBCT), 3D images of patients became more available in dentistry, with reduced radiation doses compared with multidetector computed tomography and lower costs than magnetic resonance imaging.¹¹⁻¹³ A study by Ludlow and Walker¹⁴ reported that the effective dose of radiation of CBCT for a cephalometric scan with low-dose settings may be reduced to the level of a panoramic examination at the expense of lower image quality expressed in the signal:noise ratio. However, the image quality of low-dose protocols in relation to diagnostic tasks needs to be further studied before CBCT can be recommended as a routine radiographic method for orthodontic patients.

Interest in using CBCT to measure airway volume on craniofacial growth and airway changes after orthognathic surgery and rapid maxillary expansion is growing.¹⁵⁻¹⁹ However, during the orthodontic treatment period, more lateral cephalograms are readily available than CBCT images. Previous studies have tried to find correlations between measurements performed on lateral cephalograms and CBCT images. Sears et al²⁰ measured the nasopharynx (NP), oropharynx, and hypopharynx airways, using both cephalograms and CBCT, but the correlations between linear measurements and volumes were weak. In another study, a moderately high correlation was found between the NP area on lateral cephalograms and the NP volume on CBCT images.²¹ There is no consensus concerning whether the measurements on lateral cephalograms can estimate the airway volume calculated on CBCT images.

It has been generally accepted that despite many limitations, lateral cephalograms serve as radiographic standards for airway assessment. When lateral cephalograms are used, the adenoidal nasopharyngeal ratio (ANR) is a helpful diagnostic parameter for assessing nasopharyngeal obstruction. The ANR is a classic method for assessing adenoid size in clinical diagnosis and treatment. In 1979, Fujilka et al²² obtained the ANR by simple linear measurements on the lateral radiographs of 1398 infants and children. They concluded that the ANR reliably expressed adenoidal size and patency of the nasopharyngeal airway. After that study, several reports confirmed the positive correlations between the ANR and surgical findings,²³ nasal endoscopic examinations,²⁴ and clinical symptomatology.²⁵

The size of the adenoids has an important role in the evaluation of airway volume. The adenoids develop progressively, with their growth peak reached by 4 to 5 years of age, followed by another peak between 9 and 10 years; then the size diminishes progressively until 14 to

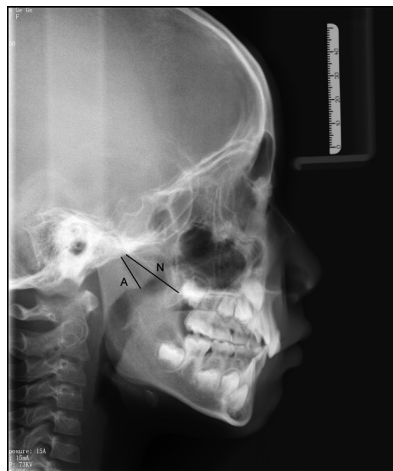


Fig 1. Linear measurements used to calculate the ANR on lateral cephalograms: A, perpendicular distance between the point of maximum convexity of the adenoid shadow to the anterior margin of the basiocciput; N, distance between the posterosuperior edge of the hard palate and the anteroinferior edge of the spheno-occipital synchondrosis.

15 years.²² Our hypothesis was that instead of linear measurement of the adenoids, the ANR on lateral cephalograms might be an applicable method to assess airway volume for younger patients.

The aim of this study was to evaluate whether the ANR on lateral cephalograms can be used to estimate the airway volume, using CBCT as the validation method. Since lateral cephalograms are routinely used in orthodontic diagnosis and treatment planning, these results will provide essential information on the value of lateral cephalograms for the assessment of airway volume.

MATERIAL AND METHODS

This study was approved by the ethics committee of the Stomatological Hospital in Dalian, China (protocol number DLKQLL201302).

This was a retrospective study; we used the image database available at the Department of Orthodontics, Stomatological Hospital, Dalian, China. The database was searched systematically between 2010 and 2012 at the Department of Oral Radiology for patients who had both lateral cephalograms and CBCT images taken not more than 1 week apart. The field of view of the CBCT images should cover the whole upper airway with the superior border above sella turcica and the

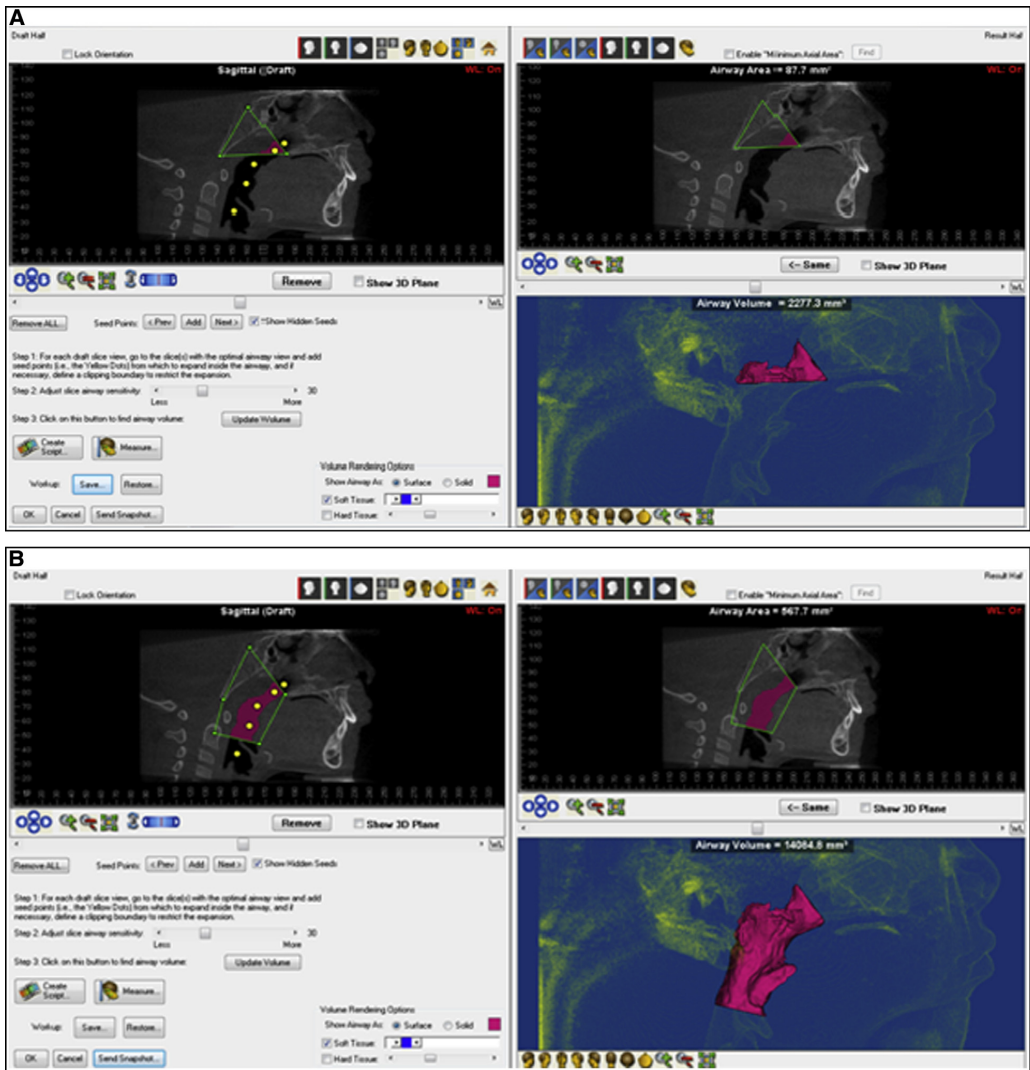


Fig 2. Airway volume and area were calculated and presented automatically after the boundaries were defined from the sagittal view (Dolphin 3D software): **A**, NP volume; **B**, total upper airway volume.

inferior border below the tip of the epiglottis. The included CBCT examinations were performed for various indications, such as temporomandibular joint disorders, orthognathic surgery, and problematic impacted teeth. Fifty-five patients (35 female, 20 male) between 9 and 43 years of age fulfilled the inclusion criteria.

All radiographs were acquired according to standard clinical exposure protocols. For lateral cephalographs, a digital pan/ceph system (ORTHOPHOS XG 5; Sirona Dental Systems, Bensheim, Germany) was used at 73 kVp and 15 mA, with exposure times of 9.7 and 9.4 seconds for adults and children, respectively. The magnification factor was 1.1 with a 16-bit pixel depth for all

images. The patients stood with the Frankfort horizontal line parallel to the floor with their teeth in maximum intercuspation.

For the CBCT examinations, a machine (3D eXam; KaVo, Biberach an der Riss, Germany) was used at 120 kV and 5 mA, with a scanning time of 14.7 seconds for the adults and children according to the manufacturer's guidelines. The voxel size was 0.2 mm, with 14-bit pixel depth for all the images, and the field of view varied depending on the purpose of the examination. The patients were asked to sit up straight with the Frankfort horizontal line parallel to the floor with their teeth in maximum intercuspation.

All images were stored in DICOM format.

Radiographs from the 55 patients were randomly arranged in 2 sequences: lateral cephalograms and CBCT images. The ANR was measured on the lateral cephalograms using the software SIDEXIS XG (Sirona Dental Systems) according to the method described by Fujioka et al²² (Fig 1). Figure 1, A denotes the perpendicular distance between the points of maximal convexity of the adenoid shadow and the anterior margin of the basiocciput. *N* is the distance between the posterosuperior edge of the hard palate and the anteroinferior edge of the sphenoid-occipital synchondrosis.

All measurements were made by 1 examiner (X.F.) under identical viewing conditions in a room with dimmed light. The CBCT images were imported as DICOM data to imaging software (version 11.0; Dolphin Imaging & Management Solutions, Chatsworth, Calif). Once the image was properly oriented, the software created a 2-dimensional simulated lateral cephalometric image at the midsagittal plane. From this view, the airway of interest could be defined using the airway analysis tool. In our study, the NP was defined with the superior border at a line connecting the midpoint of sella turcica and the posterior nasal spine, and with the inferior border at a line connecting the point most posteroinferior on the clivus with the posterior nasal spine. For the total airway volume, the superior border was the same as the NP, and the lower border of the airway was defined at a horizontal level with the tip of the epiglottis against the wall of the posterior airway.^{20,26} Data of airway volume and area in the midsagittal view could be calculated and presented automatically once the boundary of the airway was defined (Fig 2). When the airway had been demarcated by the software, the volume of the airway could be further adjusted manually at different threshold levels to ensure a more accurate representation of the airway in the head and neck regions. In our study, threshold values of 25, 30, 40, and 50 were applied for all CBCT images, and the

Table I. Calculated mean values for NP and total airway areas and volumes of each threshold

Threshold value	NP area (mm ²)	Total area (mm ²)	NP volume (mm ³)	Total volume (mm ³)
25	161.20	720.85	4649.96	18065.35
30	175.07	731.74	4793.05	18580.21
40	180.04	744.45	5012.03	19434.37
50	185.09	762.00	5216.00	21189.35
P value	0.61	0.73	0.45	0.23

ANOVA was used to compare the measurements with different thresholds.

measurements of airway areas and volumes of the midsagittal section with different thresholds were subsequently compared.

To evaluate the reliability of the ANR measurements on the cephalograms and the NP volumes on the CBCT images, the above-mentioned measurements were repeated by 2 observers (X.F., Z.Q.) on 10 randomly chosen subjects.

Statistical analysis

SPSS software (version 17.0; SPSS, Chicago, Ill) was used for data analysis. The patients were classified into 2 groups according to age: group A (≤ 15 years) and group B (> 15 years). The mean ages and standard deviations of the 2 groups were calculated. Analysis of the CBCT radiographs was performed using the following 4 parameters: NP area, NP volume, total upper airway area, and total upper airway volume. These measurements were made at the threshold levels of 25, 30, 40, and 50 provided by the software, to discriminate the airway boundaries and remove any visible extraneous scatter, artifact, or background.²⁷ The influence of the threshold levels on image analysis was analyzed using analysis of variance (ANOVA). The method repeatability of the measurements was tested in terms of intraobserver and interobserver correlation coefficients.

Correlations between the ANR values obtained from cephalograms and the measured data from the CBCT images, including the area and volume of the NP, as well as the area and volume of the total upper airway, were analyzed using scatter plots to calculate the correlation coefficients for the 2 groups.

RESULTS

Among the 55 patients, 32 were included in group A and 23 in group B. The mean ages and standard deviations of these groups were 11.8 (1.6) and 21.1 (5.7) years, respectively. For the image analyses performed

Table II. Descriptive analysis with means and standard deviations for groups A (age ≤ 15 years) and B (age > 15 years) (3D measurements with threshold 30)

	Age (y)	ANR	NP area (mm ²)	Total area (mm ²)	NP volume (mm ³)	Total volume (mm ³)
Mean (SD) group A (n = 32)	11.81 (1.59)	0.49 (0.16)	139.47 (68.91)	673.10 (202.58)	4095.0 (1928.15)	16334.96 (7220.58)
Mean (SD) group B (n = 23)	21.09 (5.74)	0.30 (0.12)	226.03 (125.32)	813.31 (174.16)	5696.55 (1346.11)	21704.02 (6810.72)

on the CBCT radiographs, no statistically significant difference was found between the measurements with different thresholds with ANOVA ($P > 0.05$) (Table I). However, the measurements had a tendency to decline as the threshold values decreased. Subsequently, a subjective viewing of all reconstructed airway volumes was conducted, and a threshold level of 30 was selected for further analyses. The means of NP area, NP volume, total upper airway area, and total upper airway volume at threshold 30 for the 2 groups are shown in Table II. The mean values of the ANR obtained from the cephalograms were 0.49 and 0.3 for groups A and B, respectively. For the repeated measurements of the ANR and NP volume, high correlation coefficient values were obtained within and between the 2 observers, indicating that both measurements were reliable (Table III). The correlation coefficient calculated by scatter plots between the ANR values from cephalograms and the measurements from CBCT are presented in Table IV. The correlation coefficients between the ANR and the NP volumes were -0.78 and -0.57 for groups A and B, respectively. Figure 3 shows the scatter plots of correlations between measurements on the cephalograms and CBCT images for the 2 age groups. Both groups exhibited a low correlation between the ANR and total upper airway area and total upper airway volume.

DISCUSSION

Many studies have reported that CBCT is an effective and accurate method to analyze airway volume.^{20,21,26,27} However, during orthodontic treatment, lateral cephalograms are more readily available than CBCT images, which are mostly taken for other diagnostic purposes. The aim of this study was to investigate whether the ANR measured on lateral cephalograms might be used to estimate airway volume.

Previous studies have used linear measurements across the airway at defined points on lateral cephalograms to evaluate NP volume, in which a weak correlation ($r = 0.43$) between the linear measurements on lateral cephalograms and the NP volume on CBCT images was found.²⁰ The difference observed between our results might be due to different measuring methods; in our study, the ANR was a ratio instead of an absolute

Table III. Observer agreement in terms of intraobserver and interobserver correlation coefficient values for repeated measurements of the ANR and NP volumes

	Intraobserver correlation coefficient		Interobserver correlation coefficient	
ANR	0.91	0.96	0.96	0.89
NP volume	0.96	0.99	0.96	0.97

Table IV. *R* values for the correlations between the ANR and 3D measurements of the groups

	ANR vs NP area	ANR vs NP volume	ANR vs total area	ANR vs total volume
Age ≤ 15 y (n = 32)	-0.77	-0.78	-0.51	-0.48
Age > 15 y (n = 23)	-0.18	-0.57	-0.30	-0.32

distance of the airway. In addition to the measuring parameter used, the airway volumes made by different imaging softwares might also to some extent influence the results because the airway volume assessment depends on the accuracy of segmentation, image quality, and the threshold interval.²⁸ In our study, the thresholds were selected to discriminate the airway boundaries and remove any visible extraneous scatter, artifact, or background.²⁷ We found that when the threshold was less than 25 (threshold of 15) or more than 50 (threshold of 60), the outline of the airway would then be visually deformed (Fig 4). Thus, thresholds at 25, 30, 40, and 50 were tested for the measurements, and no statistically significant difference among the measurements was observed. However, when the comparisons are made before and after orthodontic treatment on the same patient, the same threshold is recommended. Aboudara et al²¹ reported a correlation coefficient of 0.75 between the NP midsagittal area on lateral head films and the NP volume using CBCT. Similar values in group A ($r = -0.78$) and group B ($r = -0.57$) were found between the ANR and NP volumes in our study.

Based on our study, the ANR might be applied for analysis of the NP volume for younger patients. However, the correlations between the ANR and the area and volume of the total upper airway were dramatically

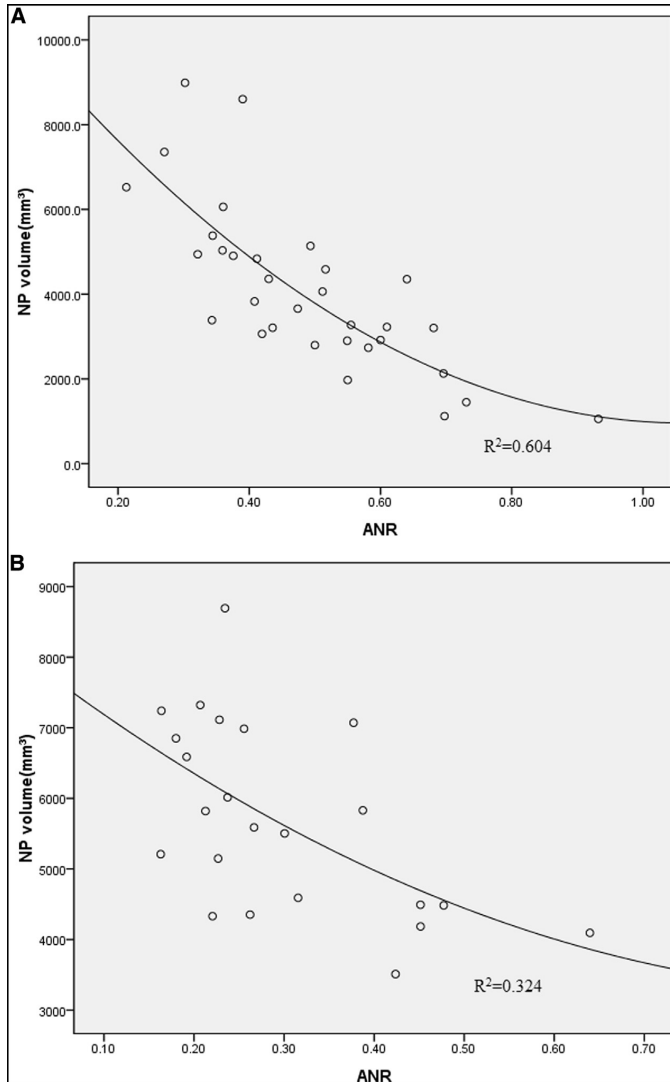


Fig 3. Scatter plots of the correlations between the ANR and NP volume: **A**, group A (age ≤15 years); **B**, group B (age >15 years).

reduced. The area and volume of the total upper airway are affected by many factors, such as length of the airway, thickness of the soft palate, axial area of the airway, and the patient's position.^{29,30} For the NP part of the airway, the size of the adenoids seems to be the most important factor; thus, the ANR is a reliable approach to simply represent the volume of

the NP. It has been reported that after 20 years of age, the soft palate becomes longer and thicker, the airway narrows, and the vertical pharyngeal length increases.³¹ Furthermore, the size and shape of the airway are known to vary during the respiratory cycle. However, in this retrospective study, the patients were not instructed to hold their breath during the scanning

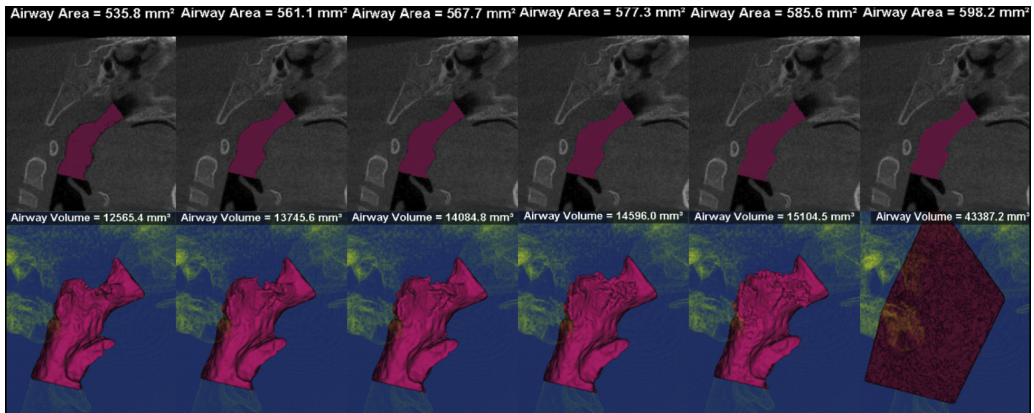


Fig 4. Reconstructed 3D airways at thresholds of 15, 25, 30, 40, 50, and 60, respectively.

time; this might have affected our measurements of total airway volume.

Since the size of the adenoids diminishes progressively and tends to be stable at age 14 to 15 years, we therefore divided the subjects into 2 groups at 15 years of age.²² According to our results, the ANR value was higher in group A than in group B, and the values of NP area, NP volume, total upper airway area, and total upper airway volume were lower in group A than in group B. In Figure 3, A, the R^2 value of 0.60 indicated that 60% of the NP volume was directly accounted for by knowing the ANR, and 40% of the variability remains unaccounted for when using lateral cephalograms to estimate the NP airway volume. Our results indicated that for younger patients, the size and morphology of the adenoids mostly affected the NP volume. For group B (Fig 3, B), the correlation coefficient value was reduced dramatically, implying that other dominant factors affect the volume of the airway other than the ANR values. However, this finding does not in any way indicate that the lateral cephalogram provides satisfactory diagnostic information for diagnosis of airway obstruction. It might be used as a screening tool to determine the need for further otolaryngologic examination. Therefore, other diagnostic tools should be recommended when the primary diagnostic task is to evaluate the airway problem.^{32,33}

CONCLUSIONS

Based on our results, measurement of the ANR on lateral cephalograms may be used as an initial screening method to estimate the NP volumes of younger patients

(≤ 15 years) throughout orthodontic treatment when lateral cephalograms are readily available.

REFERENCES

1. Abramson Z, Susarla SM, Lawler M, Bouchard C, Troulis M, Kaban LB. Three-dimensional computed tomographic airway analysis of patients with obstructive sleep apnea treated by maxillo-mandibular advancement. *J Oral Maxillofac Surg* 2011;69:677-86.
2. McCrillis JM, Haskell J, Haskell BS, Brammer M, Chenin D, Scarfe WC, et al. Obstructive sleep apnea and the use of cone beam computed tomography in airway imaging: a review. *Semin Orthod* 2009;15:63-9.
3. Solow B, Siersbaek-Nielsen S, Greve E. Airway adequacy, head posture, and craniofacial morphology. *Am J Orthod* 1984;86:214-23.
4. Capitanio MA, Kirkpatrick JA. Nasopharyngeal lymphoid tissue. Roentgen observations in 257 children two years of age or less. *Radiology* 1970;96:389-91.
5. Oulis CJ, Vadiakas GP, Ekonomides J, Dratsa J. The effect of hypertrophic adenoids and tonsils on the development of posterior crossbite and oral habits. *J Clin Pediatr Dent* 1994;18:197-201.
6. Dunn GF, Green LJ, Cunat JJ. Relationships between variation of mandibular morphology and variation of nasopharyngeal airway size in monozygotic twins. *Angle Orthod* 1973;43:129-35.
7. Feres MF, Hermann JS, Cappellette M Jr, Pignatari SS. Lateral x-ray view of the skull for the diagnosis of adenoid hypertrophy: a systematic review. *Int J Pediatr Otorhinolaryngol* 2011;75:1-11.
8. Kolo ES, Salisu AD, Tabari AM, Dahilo EA, Aluko AA. Plain radiographic evaluation of the nasopharynx: do raters agree? *Int J Pediatr Otorhinolaryngol* 2010;74:532-4.
9. Cappabianca S, Iaselli F, Negro A, Basile A, Reginelli A, Grassi R, et al. Magnetic resonance imaging in the evaluation of anatomical risk factors for pediatric obstructive sleep apnoea-hypopnoea: a pilot study. *Int J Pediatr Otorhinolaryngol* 2013;77:69-75.
10. Chi L, Comyn FL, Mitra N, Reilly MP, Wan F, Maislin G, et al. Identification of craniofacial risk factors for obstructive sleep apnoea using three-dimensional MRI. *Eur Respir J* 2011;38:348-58.

11. Ludlow JB, Ivanovic M. Comparative dosimetry of dental CBCT devices and 64-slice CT for oral and maxillofacial radiology. *Oral Surg Oral Med Oral Pathol Oral Radiol Endod* 2008;106:106-14.
12. Chau AC, Fung K. Comparison of radiation dose for implant imaging using conventional spiral tomography, computed tomography, and cone-beam computed tomography. *Oral Surg Oral Med Oral Pathol Oral Radiol Endod* 2009;107:559-65.
13. Loubele M, Bogaerts R, Van Dijk E, Pauwels R, Vanheusden S, Suetens P, et al. Comparison between effective radiation dose of CBCT and MSCT scanners for dentomaxillofacial applications. *Eur J Radiol* 2009;71:461-8.
14. Ludlow JB, Walker C. Assessment of phantom dosimetry and image quality of i-CAT FLX cone-beam computed tomography. *Am J Orthod Dentofacial Orthop* 2013;144:802-17.
15. Iwasaki T, Hayasaki H, Takemoto Y, Kanomi R, Yamasaki Y. Oropharyngeal airway in children with Class III malocclusion evaluated by cone-beam computed tomography. *Am J Orthod Dentofacial Orthop* 2009;136:318.e1-9:discussion 318-9.
16. Zhao Y, Nguyen M, Gohl E, Mah JK, Sameshima G, Enciso R. Oropharyngeal airway changes after rapid palatal expansion evaluated with cone-beam computed tomography. *Am J Orthod Dentofacial Orthop* 2010;137(Suppl):S71-8.
17. El H, Palomo JM. Measuring the airway in 3 dimensions: a reliability and accuracy study. *Am J Orthod Dentofacial Orthop* 2010;137(Suppl):S50.e1-9:discussion S50-2.
18. de Souza Carvalho AC, Magro Filho O, Garcia IR Jr, Araujo PM, Nogueira RL. Cephalometric and three-dimensional assessment of superior posterior airway space after maxillomandibular advancement. *Int J Oral Maxillofac Surg* 2012;41:1102-11.
19. El H, Palomo JM. An airway study of different maxillary and mandibular sagittal positions. *Eur J Orthod* 2013;35:262-70.
20. Sears CR, Miller AJ, Chang MK, Huang JC, Lee JS. Comparison of pharyngeal airway changes on plain radiography and cone-beam computed tomography after orthognathic surgery. *J Oral Maxillofac Surg* 2011;69:e385-94.
21. Aboudara C, Nielsen I, Huang JC, Maki K, Miller AJ, Hatcher D. Comparison of airway space with conventional lateral headfilms and 3-dimensional reconstruction from cone-beam computed tomography. *Am J Orthod Dentofacial Orthop* 2009;135:468-79.
22. Fujioka M, Young LW, Girdany BR. Radiographic evaluation of adenoidal size in children: adenoidal-nasopharyngeal ratio. *AJR Am J Roentgenol* 1979;133:401-4.
23. Al Maqbali T, Al Khabouri M, Kumar S. Radiosurgical correlation of obstructive adenoids in children. *Eur Arch Otorhinolaryngol* 2011; 268:1475-8.
24. Caylakli F, Hizal E, Yilmaz I, Yilmazer C. Correlation between adenoid-nasopharynx ratio and endoscopic examination of adenoid hypertrophy: a blind, prospective clinical study. *Int J Pediatr Otorhinolaryngol* 2009;73:1532-5.
25. Cohen LM, Koltai PJ, Scott JR. Lateral cervical radiographs and adenoid size: do they correlate? *Ear Nose Throat J* 1992;71: 638-42.
26. Lenza MG, Lenza MM, Dalstra M, Melsen B, Cattaneo PM. An analysis of different approaches to the assessment of upper airway morphology: a CBCT study. *Orthod Craniofac Res* 2010;13:96-105.
27. Weissheimer A, Menezes LM, Sameshima GT, Enciso R, Pham J, Grauer D. Imaging software accuracy for 3-dimensional analysis of the upper airway. *Am J Orthod Dentofacial Orthop* 2012;142:801-13.
28. Tso HH, Lee JS, Huang JC, Maki K, Hatcher D, Miller AJ. Evaluation of the human airway using cone-beam computerized tomography. *Oral Surg Oral Med Oral Pathol Oral Radiol Endod* 2009;108: 768-76.
29. Abramson Z, Susarla S, August M, Troulis M, Kaban L. Three-dimensional computed tomographic analysis of airway anatomy in patients with obstructive sleep apnea. *J Oral Maxillofac Surg* 2010;68:354-62.
30. Battagel JM, Johal A, Smith AM, Kotecha B. Postural variation in oropharyngeal dimensions in subjects with sleep disordered breathing: a cephalometric study. *Eur J Orthod* 2002;24:263-76.
31. Johnston CD, Richardson A. Cephalometric changes in adult pharyngeal morphology. *Eur J Orthod* 1999;21:357-62.
32. Thüer U, Kuster R, Ingervall B. A comparison between anamnestic, rhinomanometric and radiological methods of diagnosing mouth-breathing. *Eur J Orthod* 1989;11:161-8.
33. Major MP, Flores-Mir C, Major PW. Assessment of lateral cephalometric diagnosis of adenoid hypertrophy and posterior upper airway obstruction: a systematic review. *Am J Orthod Dentofacial Orthop* 2006;130:700-8.

**Prediction of aerodynamic characteristics in the upper airway by the
adenoidal nasopharyngeal ratio measured on a lateral cephalogram**

Xin Feng, Yicheng Chen, Weihua Cai, Stein Atle Lie, Kristina Hellén-Halme,
Xie-Qi Shi.

Submitted manuscript



The effect of rapid maxillary expansion on upper airway morphology: a retrospective comparison of patients with a normal vs patients with an enlarged adenoid

Xin Feng, Stein Atle Lie, Kristina Hellén-Halme, Xie-Qi Shi.

Journal of Clinical Pediatric Dentistry, 2021. 45(3) doi:10.17796/1053-4625-45.3.11



The effect of rapid maxillary expansion on the upper airway's aerodynamic characteristics

Xin Feng, Yicheng Chen, Kristina Hellén-Halme, Weihua Cai, Xie-Qi Shi.

BMC Oral Health, 2021.21(1):123. doi: 10.1186/s12903-021-01488-1

RESEARCH ARTICLE

Open Access



The effect of rapid maxillary expansion on the upper airway's aerodynamic characteristics

Xin Feng¹, Yicheng Chen², Kristina Hellén-Halme³, Weihua Cai⁴ and Xie-Qi Shi^{1,3*}

Abstract

Background: The effect of rapid maxillary expansion (RME) on the upper airway (UA) has been studied earlier but without a consistent conclusion. This study aims to evaluate the outcome of RME on the UA function in terms of aerodynamic characteristics by applying a computational fluid dynamics (CFD) simulation.

Methods: This retrospective cohort study consists of seventeen cases with two consecutive CBCT scans obtained before (T0) and after (T1) RME. Patients were divided into two groups with respect to patency of the nasopharyngeal airway as expressed in the adenoidal nasopharyngeal ratio (AN): group 1 was comprised of patients with an AN ratio < 0.6 and group 2 encompassing those with an AN ratio ≥ 0.6 . CFD simulation at inspiration and expiration were performed based on the three-dimensional (3D) models of the UA segmented from the CBCT images. The aerodynamic characteristics in terms of pressure drop (ΔP), maximum midsagittal velocity (V_{ms}), and maximum wall shear stress (P_{wss}) were compared by paired t-test and Wilcoxon test according to the normality test at T0 and T1.

Results: The aerodynamic characteristics in UA revealed no statistically significant difference after RME. The maximum V_{ms} (m/s) decreased from 2.79 to 2.28 at expiration after RME ($P=0.057$).

Conclusion: The aerodynamic characteristics were not significantly changed after RME. Further CFD studies with more cases are warranted.

Keywords: Computational fluid dynamics, Upper airway, Adenoid hypertrophy, Rapid maxillary expansion

Background

Adenoid hypertrophy (AH) is a common cause of upper airway (UA) obstruction in children and adolescents. Considerable variation in AH prevalence, ranging from 27 to 80%, has been reported between countries and ages [1]. AH may cause several health issues including mouth breathing, snoring, asthma, speech problems, and obstructive sleep apnoea [2, 3]. To diagnose the degree of AH, Fujioka proposed calculating an adenoidal nasopharyngeal (AN) ratio by measuring adenoid thickness

and nasopharyngeal width on lateral radiography, a common procedure in clinics [4, 5]. An AN ratio of more than 0.6 indicates a suspected nasal obstruction [2]. Otolaryngologists usually suggest an adenoidectomy to treat severe nasal obstruction, and this has been shown to positively affect volume expansion in the nasopharynx and improve nasal breathing. However, a noticeable recurrence of nasal obstruction after adenoidectomy has been reported [6]. In order to achieve a stable outcome after an adenoidectomy, several adjunctive treatments have been suggested for patients with specific symptoms including turbinoplasty, adenotonsillectomy, and rapid maxillary expansion (RME) [7–9].

AH may cause abnormal craniofacial development such as a short cranial base, long face, small and narrow

*Correspondence: xieqi.shi@uib.no

¹ Department of Clinical Dentistry, Faculty of Medicine, University of Bergen, Årstadveien 19, 5009 Bergen, Norway
Full list of author information is available at the end of the article



© The Author(s) 2021. **Open Access** This article is licensed under a Creative Commons Attribution 4.0 International License, which permits use, sharing, adaptation, distribution and reproduction in any medium or format, as long as you give appropriate credit to the original author(s) and the source, provide a link to the Creative Commons licence, and indicate if changes were made. The images or other third party material in this article are included in the article's Creative Commons licence, unless indicated otherwise in a credit line to the material. If material is not included in the article's Creative Commons licence and your intended use is not permitted by statutory regulation or exceeds the permitted use, you will need to obtain permission directly from the copyright holder. To view a copy of this licence, visit <http://creativecommons.org/licenses/by/4.0/>. The Creative Commons Public Domain Dedication waiver (<http://creativecommons.org/publicdomain/zero/1.0/>) applies to the data made available in this article, unless otherwise stated in a credit line to the data.

maxilla, and mandibular retrusion [10–12]. Some orthodontists suggest that RME may have the potential to reduce nasal obstruction by opening the midsagittal suture, widening the maxillary arch, and increasing nasal space [9, 13, 14].

RME's possible effect on nasal obstruction has been evaluated by several methods including rhinomanometry, acoustic rhinometry, polysomnography (PSG), cephalometric radiographs, cone beam computed tomography (CBCT) and computed tomography (CT), but with inconsistent conclusions [15, 16]. Laboratory-based PSG is considered the gold standard for diagnosing obstructive sleep apnoea, as it provides quantitative parameters to evaluate respiratory function such as the apnoea–hypopnea index [17]. However, it also has limited availability and is relatively expensive and time consuming, which could be inconvenient for children and their families. Therefore, researchers have been searching for alternative methods to evaluate the respiratory function of UA. For example, De Backer et al. [18] introduced computational fluid dynamics (CFD) as a diagnostic tool to observe the outcome of mandibular advancement devices when treating sleep-related breathing disorders and found that CFD models precisely capture UA's aerodynamic characteristics. Moreover, the CFD results show a higher correlation with clinical symptoms than volumetric measurements on CT images.

The CFD method is a well-established technique that has been widely used in mechanical engineering, yet it is quite new to flow analysis in medicine. Based on a three-dimensional (3D) structure segmented from CBCT, CT, or magnetic resonance imaging (MRI), the CFD simulates and calculates the flow of gases or fluids and their interactions with the surrounding surfaces as defined by boundary conditions. At a given inlet pressure, the shape and boundary condition of a pipe-like UA would theoretically determine the aerodynamic characteristics in terms of pressure, velocity, and wall shear stress. The application of CFD in dentistry is nevertheless sparse. Few previous studies have shown that CFD could be applied to evaluate the outcome of mandible advanced devices on respiratory function [18, 19]. Regarding the effect of RME on airflow within the UA, Iwasaki et al. observed an improvement in nasal cavity obstruction [20] and a decrease in pharyngeal airway pressure after RME [21]. More clinical evidence on the changes of UA following RME is, however, needed to enhance and benefit individual treatment planning for patients with a narrow maxilla and enlarged adenoid.

In this study, we aim to evaluate the effect of RME on airflow within the UA by investigating the aerodynamic characteristics that result from applying CFD simulation.

The null hypothesis is that RME has a positive effect on UA ventilation.

Methods

This is a retrospective cohort study. All methods were carried out in accordance with the declaration of research involving human subjects and the regional ethical and scientific guidelines in Vestland region, Norway. Data for all patients who had undergone RME were retrospectively collected at the Department of Orthodontics (Stomatological hospital, Dalian, China) between January 2013 and December 2016. The inclusion criteria were patients younger than 15 years old who had both pre- and post-CBCT scans due to orthodontic indication. The pre-RME CBCTs were taken within seven days prior to fixing the expander (T0) and the post-RME CBCTs at the removal of expanders (T1). The exclusion criteria were severe abnormalities of maxillofacial tissue, previous surgery on skeletal and soft tissue related to respiration, and previous orthodontic or orthopaedic treatment. Eventually, 17 patients (mean age 12.2 ± 1.3 years, 11 male/6 female) were eligible for inclusion in the study. An experienced radiologist viewed all CBCT scans and ensured that the images were qualified to construct 3D models of the UA.

Maxillary expansion protocol

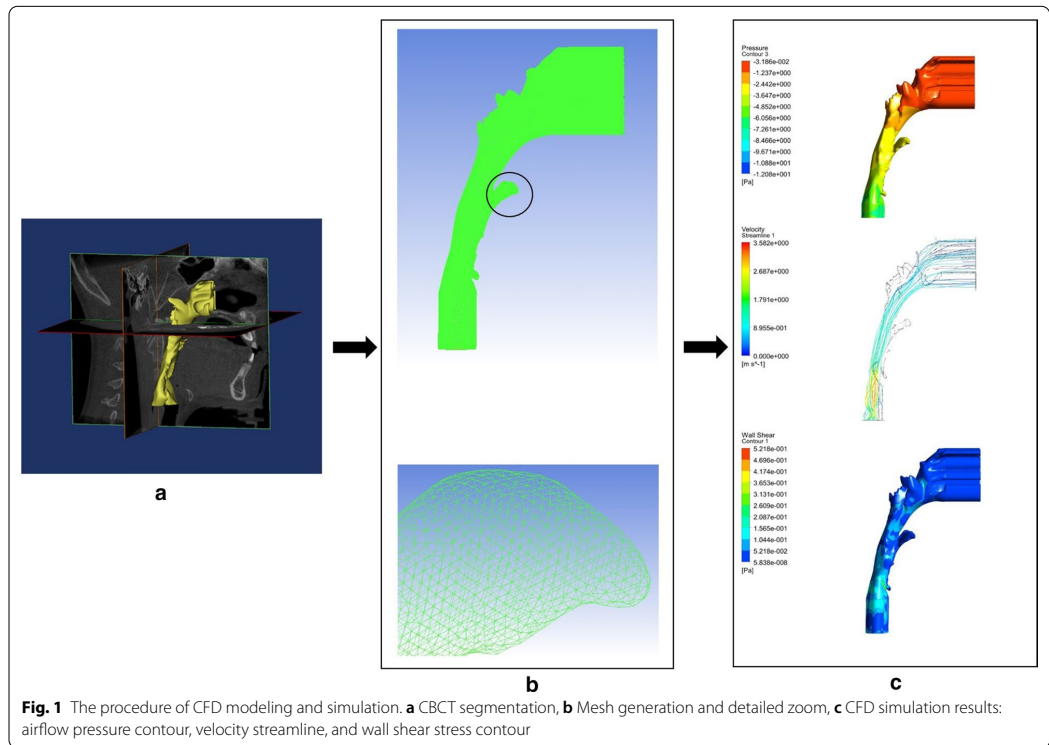
A fixed Hyrax expander was used for RME, banded to the maxillary first premolars and first molars. The patient, or their guardian, rotated the expansion screw twice a day at home and a clinical check-up was performed by orthodontists once a week. The expansion was terminated when the occlusal aspect of the maxillary lingual cusps of the upper first molars contacted the occlusal aspect of the vestibular cusp of the mandibular first molars. After achieving the desired expansion, the expander remained in place for 5.2 ± 1.7 months to stabilise the expansion.

CFD simulation

Figure 1 demonstrates the stepwise procedure of the CFD modelling and simulation, including 3D segmentation, mesh generation, and aerodynamic results.

CBCT imaging

The examination protocol of CBCT scans was as follows: field of view (FOV) 16×13 cm; tube potential 120 kVp and tube current 5 mA; scanning time 14.7 s (3D eXam; KaVo, Biberach an der Riss, Germany). The voxel size was set at 0.2 mm, and the contrast resolution had a 14-bit depth. All CBCT examinations were performed according to the standardised clinical routine, i.e. with the Frankfort horizontal plane parallel to the floor, teeth in maximum intercuspation, and peaceful nasal breathing



without swallowing. We divided the 17 patients into two groups according to the AN ratio at baseline (T0): group 1 was comprised of individuals with an AN ratio < 0.6 and group 2 encompassing those with an AN ratio ≥ 0.6 . The measurements of AN ratios were performed aiming to present the geometric obstruction status of the UA following Fujioka's method [4]. A and N indicated the adenoid thickness and nasopharyngeal width, respectively (Fig. 2). The CBCT images were imported to MIMICS software (Materialise Mimics 23.0, Belgium) in the digital imaging and communications in medicine (DICOM) format for later analysis. To segment the 3D UA, one author (XF) orientated the CBCT image. An appropriate threshold was set from -1024 to -500 to involve the UA without deflection [22], which was called a "mask". The superior boundary was defined on the mask as perpendicular to the horizontal plane through the most posterior point of middle turbinate in the sagittal view; the inferior boundary was parallel to the horizontal plane through the most anterior–inferior point of cervical vertebra 4. The 3D UA was then calculated from the

defined mask. The superior and inferior boundaries were extended by 20 mm to avoid flow reversing [23]. The extended 3D model was used to create a surface model for further mesh generation.

Mesh generation

Mesh generation is the practice of creating a mesh by computer algorithms. The continuous geometric UA space may be subdivided into discrete geometric cells. Mesh cell is the fundamental element of the reconstructed space that contains a local approximation of aerodynamic characteristics, which will be used for a later calculation. We chose tetrahedral and prismatic cells to construct the main body and boundary layer of the UA (ANSYS, Inc., Canonsburg, Pennsylvania). Each UA mesh had five boundary layers and an average of 2 million elements. The inlet and outlet of UA were defined at the extended superior and inferior boundary, as earlier described.

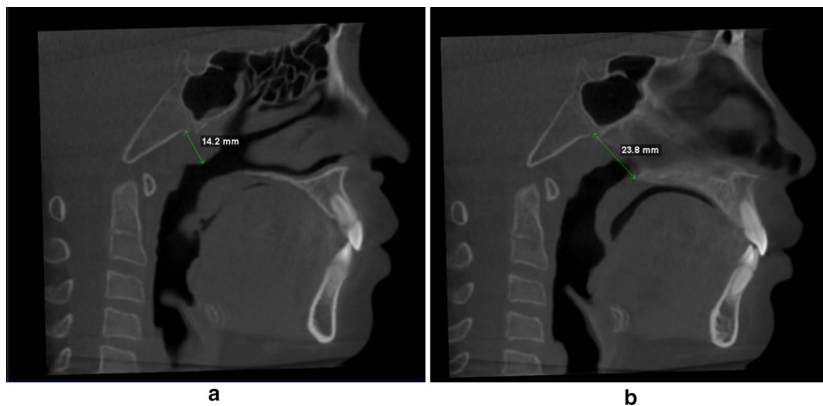


Fig. 2 The measurement of AN ratio on CBCT images. **a** A, perpendicular distance from the maximal convexity of the adenoid identifying by scrolling through the sagittal slice that showed maximal convexity of the adenoid (where the intersecting axial view also showed maximal convexity) to the anterior margin of the basiocciput. **b** N, distance between the posterosuperior point of the hard palate and the anteroinferior point of the spheno-occipital synchondrosis on the mid-sagittal plane

Aerodynamic analysis

ANSYS Fluent (ANSYS, Inc.) was applied to simulate the airflow of UA, and the SST κ - ω model was used to calculate the aerodynamic characteristics of UA. The wall of UA was defined as no-slip, stationary, and rigid, and the temperature and density of air were set as fixed [24]. In the inspiratory phase, the inlet was set with pressure 0 Pa and the outlet a flow rate of -200 mL/s [20]. The corresponding values were -200 mL/s and 0 Pa at inlet and outlet for the expiratory phase. Over 2000 iterations were performed to ensure the resulting residuals were less than 10^{-6} . A radiologist (XF) performed all the simulations under the technical supervision of a fluid engineer (YCC). The CFD simulations were repeated six months later on ten randomly selected cases by the same operator (XF).

Data analyses

We calculated the aerodynamic characteristics at inspiratory and expiratory phases, including mean pressure at the four planes defined on UA (Fig. 3). The parameters included are the pressure drop (ΔP) from plane 1 to plane 4, the maximum mid-sagittal velocity (V_{ms}), and maximum wall shear stress (P_{ws}) at T0 and T1. Data were processed using the IBM-SPSS version 25.0 (IBM, New York, NY, USA). Significance was set at p less than 0.05. Statistical tests for normality were conducted for all variables. Accordingly, paired t -test or Wilcoxon test was used to compare the changes of the aerodynamic characteristics between T0 and T1. Intraclass Correlation Coefficient

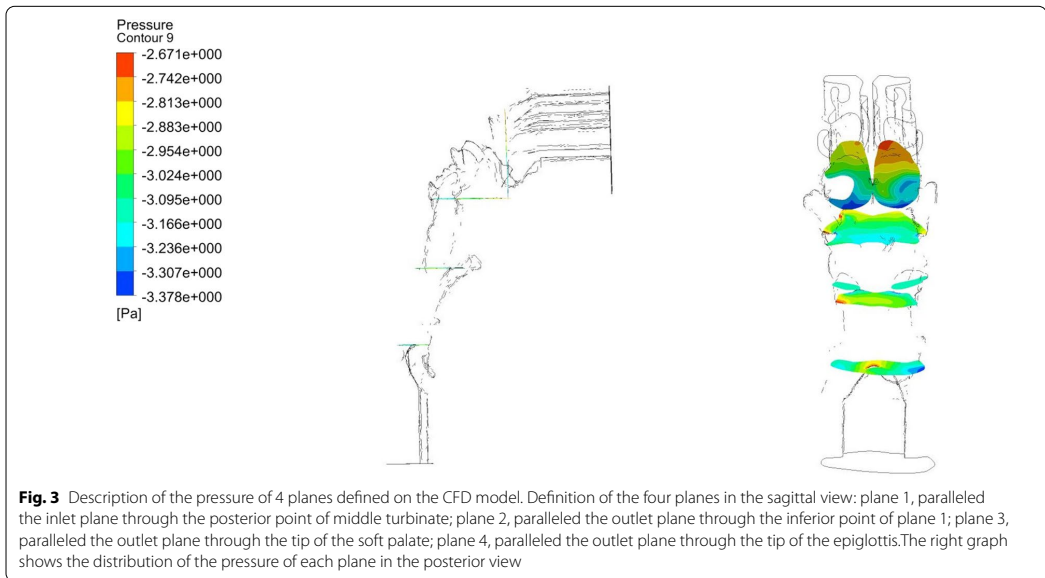
(ICC) was applied to test the consistency of the CFD simulations.

Results

The comparison of aerodynamic characteristics in terms of ΔP , the maximum V_{ms} and maximum P_{ws} of the UA between before (T0) and after (T1) RME were shown in Table 1. The ICC ranged between 0.787 and 1 for all measurements indicating the high repeatability of CFD method.

Among the 17 patients, ten patients were classified in group 1 (mean age 11.9 ± 1.3 years); seven patients in group 2 (mean age 12.6 ± 1.3 years). Figure 4 illustrates the distributions of the aerodynamic variables for the two groups at T0 and T1 graphically. It demonstrates that group 2 has higher mean ΔP and mean V_{ms} than group 1 at both inspiration and expiration regardless of T0 or T1; whereas the maximum P_{ws} shows the opposite trend being lower for group 2.

Due to the limited number of cases, group 1 and group 2 were merged when performing the statistical analysis on the effect of RME. Except for ΔP at inspiration, all the other aerodynamic parameters decrease after RME treatment (Table 1). However, none of the changes is statistically significant, of which the V_{ms} (m/s) drop (2.79 – 2.28) at expiration is close to being significant ($p=0.057$).



Discussion

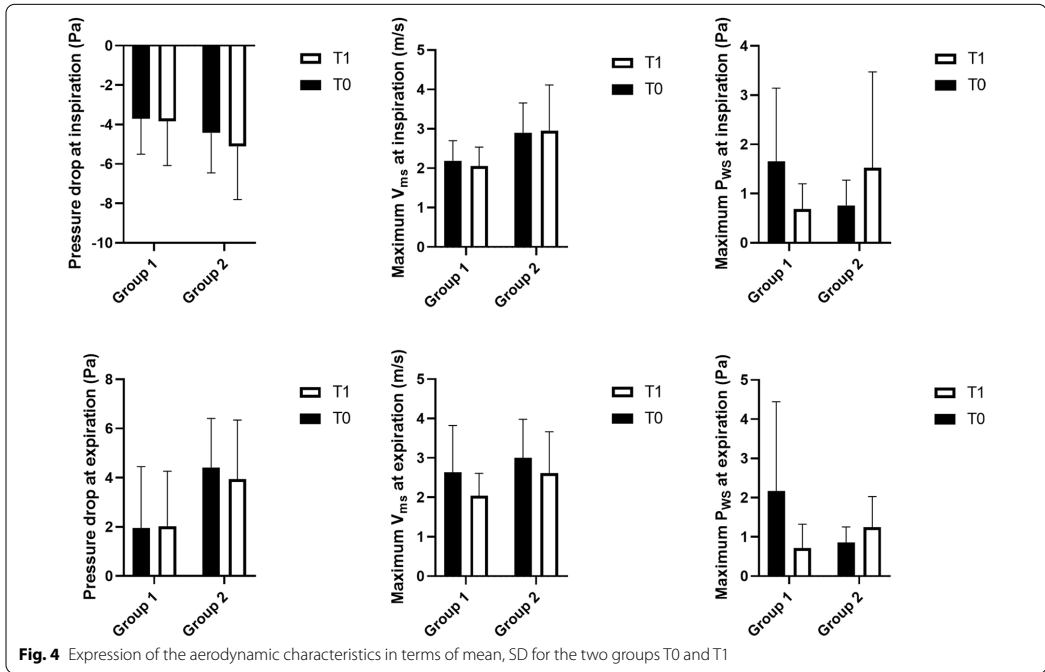
CFD simulation

In the engineering field, the pressure drop is defined as the pressure difference between two points of a fluid carrying network, which occurs when frictional forces, caused by the resistance to flow, interact with fluid as it flows through the tube. Applying this concept to airflow passing through the UA, the pressure drops when facing physical force caused by morphological changes. Furthermore, the maximum V_{ms} may be altered following

UA morphological changes. Faramarzi et al. evaluated the aerodynamics of the nasal cavity in a patient with septal perforation and found higher velocity at areas with higher pressure drop [25]. Regarding wall shear stress, it expresses the force per unit area exerted by the wall on the fluid in a direction on the local tangent plane [26]. The maximum P_{ws} locates mostly at a constricted area [27]. A successful expansion of maxilla suture would hypothetically increase the UA space, resulting in declines in ΔP , maximum V_{ms} and maximum P_{ws} .

Table 1 Comparison of pressure drop (ΔP), maximum midsagittal velocity (V_{ms}), and maximum wall shear stress (P_{ws}) at inspiration and expiration before (T0) and after (T1) rapid maxillary expansion (n = 17)

	T0		T1		T0 versus T1	
	Mean	SD	Mean	SD	p value	
					Paired t test	Wilcoxon test
<i>Inspiration</i>						
ΔP (Pa)	-4.00	1.87	-4.36	2.45	0.549	
Maximum V_{ms} (m/s)	2.48	0.70	2.43	0.92	0.906	
Maximum P_{ws} (Pa)	1.29	1.24	1.03	1.32	0.163	
<i>Expiration</i>						
ΔP (Pa)	2.96	2.56	2.81	2.43	0.943	
Maximum V_{ms} (m/s)	2.79	1.09	2.28	0.82	0.057	
Maximum P_{ws} (Pa)	1.63	1.85	0.93	0.71	0.381	



In the present study, CFD simulation was applied to elucidate the aerodynamic characteristics of the UA before and after RME. The null hypothesis was rejected, i.e. RME does not have a positive effect on UA ventilation. We failed to observe any statistically significant change in airflow characteristics after RME despite overall declines of ΔP , maximum V_{ms} and maximum P_{ws} . The difference in V_{ms} after RME (2.79–2.28) at expiration is nearly significant ($p=0.057$). This finding is in line with previous reports where the airflow resistance at expiration was found to be closely related to obstructive severity [28, 29]. Also, Chen et al. reported that patients with obstructive sleeping problem had a higher airflow resistance during the expiratory phase than the healthy subjects applying by CFD simulation [30].

The effect of RME on aerodynamics has been investigated sparsely. In contrast to the present study, Iwasaki et al. found significant changes in aerodynamic characteristics in the nasal cavity after RME [21]. This may imply that the RME mainly increases the maxilla width in the transverse direction and the skeletal boundary of nasal cavity was directly extended following with the expanded maxilla [20]. The pharyngeal part of UA is surrounded by multiple soft tissues and located posteriorly

to the maxilla. Thus the positive effect of RME on UA is more notable in the nasal cavity than the lower UA region. More cases are needed to detect possible effect and to increase the power of the applied statistics.

Enlarged adenoid is a common cause of nasal obstruction in children. Knowledge of aerodynamics in this group of patients would help understand the disease mechanism, assist diagnostics and evaluate treatment outcomes. Due to the small sample size, we did not perform statistical analysis on the effect of RME for each individual group. Nevertheless, ΔP and maximum V_{ms} seemed to be lower in group 1 as compared to group 2 regardless of T0 or T1 (Fig. 4), indicating air resistance in UA seemed to be higher in patients with enlarged adenoids. However, we are puzzled by the results of the maximum P_{ws} .

It has been reported that one of the most restricted areas in UA was located at the velopharynx where the maximum P_{ws} and a pharyngeal jet were observed [31, 32]. In our case, we speculate that an “adenoid jet” might have occurred when airflow passing through the enlarged adenoid (group 2). The high-speed adenoid jet might have caused strong vortexes and a complex recirculation resulting in a retarded downstream velocity gradient

near UA's wall and thus a reduced maximum P_{ws} . Consequently, the maximum P_{ws} was lower in group 2 than group 1 at T0. After RME the adenoid jet may be weakened, resulting in an increased maximum P_{ws} in group 2. However, due to limited cases and the diverse airflow characteristics in group 2, random effect can not be excluded. Therefore, more cases with severely enlarged adenoids are needed to confirm our assumption.

CFD is a valuable tool for investigating the aerodynamic characteristics of the UA for better understanding the complex airflow ventilation related to UA morphology. At present, the simulation procedure is not entirely automatic and thus very time consuming. Part of the 3D segmentation and mesh generation needs to be performed manually due to the irregular anatomic structure of the UA. This may be the cause for the limited number of samples in the available CFD studies [19, 33, 34]. However, we do believe, with the help of artificial intelligence the CFD simulation procedure could be simplified and less time consuming in the near future.

Clinical implications

The CFD method makes the aerodynamic characteristics within the UA visible. However, due to the intrinsic nature of a retrospective study design, the lack of clinical otolaryngologic examination makes it difficult to conclude whether RME would affect the airflow condition. Nevertheless, the enlarged adenoid may influence the UA's ventilation. Further perspective study is warranted to identify the specific patients who may benefit from the RME.

Conclusions

The aerodynamic characteristics were not significantly changed after RME. Further CFD studies with more cases are warranted.

Acknowledgements

Not applicable.

Authors' contributions

XF contributed to design, data acquisition, image segmentation, CFD simulation, and interpretation, drafted and critically revised the manuscript. YCC contributed to the study design and supervised the CFD simulation process. KH-H contributed to conception, design, and supervised manuscript writing. WHC contributed to conception and design with respect to CFD simulation. X-QS contributed to conception, design, data interpretation, and critically revised the manuscript. All authors commented on all drafts of the manuscript. All authors read and approved the final manuscript.

Funding

This work was supported by grants provided by Dalian Medical Science Project, China (No. 1611079) as well as grants provided by University of Bergen, Norway (SPIRE project). The funding body was not involved in the study design, data collection, data analysis, or interpretation of data, or in writing the manuscript.

Availability of data and materials

All data used and/or analysed during the current study are available from the corresponding author on reasonable request.

Declarations

Ethics approval and consent to participate

The study was approved by the ethics committee of China (DLKQLL201604, Dalian Stomatological Hospital) as well as the ethics committee of Norway (2018/1547 REK Vest, University of Bergen). Written informed consent was obtained from all participants or their legal guardians.

Consent for publication

Not applicable as there are no participants' identifiable data, picture or illustrations that require consent to publish in this manuscript.

Competing interests

The authors declare that they have no competing interest.

Author details

¹ Department of Clinical Dentistry, Faculty of Medicine, University of Bergen, Årstadveien 19, 5009 Bergen, Norway. ² School of Energy Science and Engineering, Harbin Institute of Technology, Xi Da Zhi Street, Nangang 150001, Harbin, People's Republic of China. ³ Department of Oral and Maxillofacial Radiology, Faculty of Odontology, Malmö University, 205 06, Malmö, Sweden. ⁴ School of Energy and Power Engineering, Northeast Electric Power University, Changchun Road 169, Changchun 132012, Jilin, People's Republic of China.

Received: 15 December 2020 Accepted: 4 March 2021

Published online: 17 March 2021

References

- Pereira L, Monyror J, Almeida FT, Almeida FR, Guerra E, Flores-Mir C, Pacheco-Pereira C. Prevalence of adenoid hypertrophy: a systematic review and meta-analysis. *Sleep Med Rev.* 2018;38:101–12.
- Tatlipinar A, Biteker M, Meric K, Bayraktar GI, Tekkesin AI, Gokceer T. Adenotonsillar hypertrophy: correlation between obstruction types and cardiopulmonary complications. *Laryngoscope.* 2012;122(3):676–80.
- Pagella F, De Amici M, Pusateri A, Tinelli G, Matti E, Benazzo M, Licari A, Nigrisoli S, Quaglini S, Ciprandi G, et al. Adenoids and clinical symptoms: epidemiology of a cohort of 795 pediatric patients. *Int J Pediatr Otorhinolaryngol.* 2015;79(12):2137–41.
- Fujioka M, Young LW, Girdany BR. Radiographic evaluation of adenoidal size in children: adenoidal–nasopharyngeal ratio. *AJR Am J Roentgenol.* 1979;133(3):401–4.
- Duan H, Xia L, He W, Lin Y, Lu Z, Lan Q. Accuracy of lateral cephalogram for diagnosis of adenoid hypertrophy and posterior upper airway obstruction: a meta-analysis. *Int J Pediatr Otorhinolaryngol.* 2019;119:1–9.
- Mitchell RB, Archer SM, Ishman SL, Rosenfeld RM, Coles S, Finestone SA, Friedman NR, Giordano T, Hildrew DM, Kim TW, et al. Clinical practice guideline: tonsillectomy in children (update). *Otolaryngol Head Neck Surg.* 2019;160(1):S1–42.
- Chohan A, Lal A, Chohan K, Chakravarti A, Gomber S. Systematic review and meta-analysis of randomized controlled trials on the role of mome-tasone in adenoid hypertrophy in children. *Int J Pediatr Otorhinolaryngol.* 2015;79(10):1599–608.
- Baik G, Brietzke SE. Cost benefit and utility decision analysis of turbino-plasty with adenotonsillectomy for pediatric sleep-disordered breathing. *Otolaryngology Head and Neck Surgery.* 2019;161(2):343–7.
- Guilleminault C, Monteyrol PJ, Huynh NT, Pirelli P, Quo S, Li K. Adenotonsillectomy and rapid maxillary distraction in pre-pubertal children, a pilot study. *Sleep Breath.* 2011;15(2):173–7.
- Schendel SA, Eisenfeld J, Bell WH, Epker BN, Mischevich DJ. The long face syndrome: vertical maxillary excess. *Am J Orthod.* 1976;70(4):398–408.
- Macari AT, Bitar MA, Ghafari JG. New insights on age-related association between nasopharyngeal airway clearance and facial morphology. *Orthod Craniofac Res.* 2012;15(3):188–97.

12. Garetz SL, Mitchell RB, Parker PD, Moore RH, Rosen CL, Giordani B, Muzumdar H, Paruthi S, Elden L, Willging P, et al. Quality of life and obstructive sleep apnea symptoms after pediatric adenotonsillectomy. *Pediatrics*. 2015;135(2):e477–486.
13. Huynh NT, Desplats E, Almeida FR. Orthodontics treatments for managing obstructive sleep apnea syndrome in children: a systematic review and meta-analysis. *Sleep Med Rev*. 2016;25:84–94.
14. Hamoda MM, Kohzuka Y, Almeida FR. Oral appliances for the management of OSA: an updated review of the literature. *Chest*. 2018;153(2):544–53.
15. Di Carlo G, Saccucci M, Ierardo G, Luzzi V, Occasi F, Zicari AM, Duse M, Polimeni A. Rapid maxillary expansion and upper airway morphology: a systematic review on the role of cone beam computed tomography. *Biomed Res Int*. 2017;2017:5460429.
16. Kilic N, Oktay H. Effects of rapid maxillary expansion on nasal breathing and some naso-respiratory and breathing problems in growing children: a literature review. *Int J Pediatr Otorhinolaryngol*. 2008;72(11):1595–601.
17. Roland PS, Rosenfeld RM, Brooks LJ, Friedman NR, Jones J, Kim TW, Kuhar S, Mitchell RB, Seidman MD, Sheldon SH, et al. Clinical practice guideline: polysomnography for sleep-disordered breathing prior to tonsillectomy in children. *Otolaryngol Head Neck Surg*. 2011;145(1 Suppl):S1–15.
18. De Backer JW, Vanderveken OM, Vos WG, Devolder A, Verhulst SL, Verbraecken JA, Parizel PM, Braem MJ, Van de Heyning PH, De Backer WA. Functional imaging using computational fluid dynamics to predict treatment success of mandibular advancement devices in sleep-disordered breathing. *J Biomech*. 2007;40(16):3708–14.
19. Martínez A, Muñoz AL, Soudah E, Calvo J, Suárez AA, Cobo J, Cobo T. Physiological and geometrical effects in the upper airways with and without mandibular advance device for sleep apnea treatment. *Sci Rep*. 2020;10(1):5322–5322.
20. Iwasaki T, Saitoh I, Takemoto Y, Inada E, Kanomi R, Hayasaki H, Yamasaki Y. Improvement of nasal airway ventilation after rapid maxillary expansion evaluated with computational fluid dynamics. *Am J Orthod Dentofac Orthop*. 2012;141(3):269–78.
21. Iwasaki T, Takemoto Y, Inada E, Sato H, Suga H, Saitoh I, Kakuno E, Kanomi R, Yamasaki Y. The effect of rapid maxillary expansion on pharyngeal airway pressure during inspiration evaluated using computational fluid dynamics. *Int J Pediatr Otorhinolaryngol*. 2014;78(8):1258–64.
22. Rana SS, Kharbanda OP, Agarwal B. Influence of tongue volume, oral cavity volume and their ratio on upper airway: a cone beam computed tomography study. *J Oral Biol Craniofac Res*. 2020;10(2):110–7.
23. Cisonni J, Lucy AD, King AJ, Islam SM, Lewis R, Goonewardene MS. Numerical simulation of pharyngeal airflow applied to obstructive sleep apnea: effect of the nasal cavity in anatomically accurate airway models. *Med Biol Eng Comput*. 2015;53(11):1129–39.
24. Powell NB, Mihaescu M, Mylavarapu G, Weaver EM, Guillemainault C, Gutmark E. Patterns in pharyngeal airflow associated with sleep-disordered breathing. *Sleep Med*. 2011;12(10):966–74.
25. Faramarzi M, Baradaranfar MH, Abouali O, Atighechi S, Ahmadi G, Farhadi P, Keshavarzian E, Behniafar N, Baradaranfar A. Numerical investigation of the flow field in realistic nasal septal perforation geometry. *Allergy Rhinol (Providence)*. 2014;5(2):70–7.
26. Katritsis D, Kaiktsis L, Chaniotis A, Pantos J, Efsthathopoulos EP, Marmarelis V. Wall shear stress: theoretical considerations and methods of measurement. *Prog Cardiovasc Dis*. 2007;49(5):307–29.
27. Murata N, Hiro T, Takayama T, Migita S, Morikawa T, Tamaki T, Mineki T, Kojima K, Akutsu N, Sudo M, et al. High shear stress on the coronary arterial wall is related to computed tomography-derived high-risk plaque: a three-dimensional computed tomography and color-coded tissue-characterizing intravascular ultrasonography study. *Heart Vessels*. 2019;34(9):1429–39.
28. Verbraecken JA, De Backer WA. Upper airway mechanics. *Respiration*. 2009;78(2):121–33.
29. Tamisier R, Pepin JL, Wuyam B, Deschaux C, Levy P. Expiratory changes in pressure: flow ratio during sleep in patients with sleep-disordered breathing. *Sleep*. 2004;27(2):240–8.
30. Chen H, Li Y, Reiber JH, de Lange J, Tu S, van der Stelt P, Lobbezoo F, Aarab G. Analyses of aerodynamic characteristics of the oropharynx applying CBCT: obstructive sleep apnea patients versus control subjects. *Dentomaxillofac Radiol*. 2018;47(2):20170238.
31. Zhao M, Barber T, Cistulli P, Sutherland K, Rosengarten G. Computational fluid dynamics for the assessment of upper airway response to oral appliance treatment in obstructive sleep apnea. *J Biomech*. 2013;46(1):142–50.
32. Jeong S-J, Kim W-S, Sung S-J. Numerical investigation on the flow characteristics and aerodynamic force of the upper airway of patient with obstructive sleep apnea using computational fluid dynamics. *Med Eng Phys*. 2007;29(6):637–51.
33. Lambeth C, Wang Z, Kairaitis K, Moshfegh A, Jabbarzadeh A, Amis TC. Modelling mucosal surface roughness in the human velopharynx: a computational fluid dynamics study of healthy and obstructive sleep apnea airways. *J Appl Physiol*. 2018;125:1821–31.
34. Mortazavy Beni H, Hassani K, Khorramymehr S. In silico investigation of sneezing in a full real human upper airway using computational fluid dynamics method. *Comput Methods Programs Biomed*. 2019;177:203–9.

Publisher's Note

Springer Nature remains neutral with regard to jurisdictional claims in published maps and institutional affiliations.

Ready to submit your research? Choose BMC and benefit from:

- fast, convenient online submission
- thorough peer review by experienced researchers in your field
- rapid publication on acceptance
- support for research data, including large and complex data types
- gold Open Access which fosters wider collaboration and increased citations
- maximum visibility for your research: over 100M website views per year

At BMC, research is always in progress.

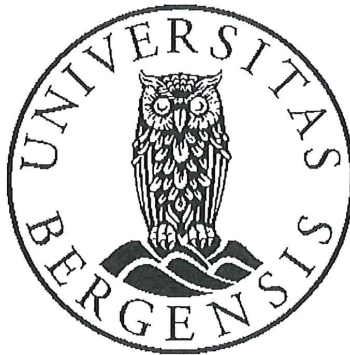
Learn more biomedcentral.com/submissions



Errata for

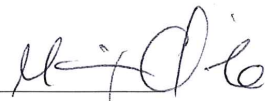
Image-based analyses of morphology and function in the upper airway of
orthodontic patients

Xin Feng



Thesis for the degree philosophiae doctor (PhD)
at the University of Bergen

18.05.2021 Xin Feng
(date and sign. of candidate)

18.05.21 
(date and sign. of faculty)

Errata

Study II

Page 14, Fig.1 legend. “The procedure of CFD modeling and simulation” corrected to “The measurement of AN ratio on lateral cephalogram”

Page 15, Fig.2 legend. “The measurement of AN ratio on CBCT images” corrected to “Comparison of aerodynamic parameters between the two groups”

Study IV

Page 11-13, References, Formatting error:

6. Mitchell RB, Archer SM, Ishman SL, Rosenfeld RM, Coles S, Finestone SA, Friedman NR, Giordano T, Hildrew DM, Kim TW et al: Clinical Practice Guideline: Tonsillectomy in Children (Update). Otolaryngology-head and neck surgery: official journal of American Academy of Otolaryngology-Head and Neck Surgery 2019, 160(1): S1-S42.

33. Lambeth C, Wang Z, Kairaitis K, Moshfegh A, Jabbarzadeh A, Amis TC. Modelling mucosal surface roughness in the human velopharynx: a computational fluid dynamics study of healthy and obstructive sleep apnea airways. J Appl Physiol. 2018,125:1821–1831.



Graphic design: Communication Division, UIB / Print: Skjipes Kommunikasjon AS



uib.no

ISBN: 9788230869109 (print)
9788230869536 (PDF)